FCP Report No. 17

THE EFFECT OF CONTACT GEOMETRY ON FRETTING FATIGUE

by

Graham Roberts
Department of Theoretical and Applied Mechanics

ABSTRACT

Some recent research literature has proposed that the initiation of fatigue cracks under fretting conditions is largely dependent on the local macroscopic stress distribution in the contact area. The work reported herein is an investigation of this theory by using contact pads of different geometries which give rise to different stress distributions.

A Report of the
FRACTURE CONTROL PROGRAM

College of Engineering, University of Illinois
Urbana, Illinois 61801
June, 1975

ACKNOWLEDGMENT

This investigation was conducted in the H. F. Moore Fracture Research Laboratory of the Department of Theoretical and Applied Mechanics, University of Illinois, Urbana. Financial support was provided by the University of Illinois Fracture Control Program, headed by Professor JoDean Morrow.

The work was conducted while the author was on secondment from the Department of Engineering Science, Plymouth Polytechnic, England.

The author is indebted to his advisor, Professor George M. Sinclair, for his suggestions, constructive criticism and encouragement. Appreciation is also expressed to Professor JoDean Morrow for his technical stimulation and friendship.

The author wishes to thank all the members of the workshop who assisted in preparing the specimens and test equipment, also Karen Hageman, Cynthia Faw, Barbara Wonneberg and Darlene Mathine for assistance in preparing the manuscript.

Finally, the author expresses thanks to his wife, Liz, and his children, Sally and Philip, for their patience during his absence.

TABLE OF CONTENTS

Chapter Page

LIST OF TABLES

LIST OF FIGURES

LIST OF SYMBOLS

a	Crack length
a_{th}	Threshold crack length
A	Fatigue crack growth coefficient
b	Fatigue strength exponent
B	Width of specimen
c	Fatigue ductility exponent
$F\left(\frac{a}{B}\right)$	Mathematical function of a/B
k	Ratio of σ_{xx}/σ_{yy}
K	Stress intensity factor
L	Half contact length
n'	Cyclic strain hardening exponent
N	Number of fatigue cycles
N_f	Number of fatigue cycles to fracture
p	Normal pressure distribution
p_{av}	Average normal pressure
r	Fatigue crack growth exponent
ΔK	Stress intensity factor range
ΔK_{th}	Threshold stress intensity factor range
ΔS	Applied cyclic stress range
ΔS_N	Applied cyclic stress range for fatigue fracture in N cycles
ΔS_{fN}	Applied cyclic stress range for fretting fatigue fracture in N cycles
$\Delta\tau$	Shear stress range
$\Delta\tau_N$	Shear stress range to cause fatigue failure in axial loading only
$\Delta\tau_{fN}$	Shear stress range to cause fretting fatigue failure

μ	Coefficient of friction
σ	Direct stress
σ_f'	Fatigue strength coefficient
σ_y	Monotonic yield stress
σ_y'	Cyclic yield stress

1. INTRODUCTION

1.1 The Fretting Phenomenon

Fretting is the term used to describe the small amplitude oscillatory slip which may occur between two components in an engineering structure that is subjected to dynamic loading. At points where relative movement occurs, the first noticeable sign of damage is the formation of a powdery deposit which resembles the metallic oxide, this is often associated with considerable wear of the surfaces. In addition, small cracks may form in the damaged area and in some cases these cracks propagate through the structure causing fatigue failure.

The first record of fretting damage is believed to be by Eden, Rose and Cunningham in 1911 [1] who observed that during fatigue tests the varying stress between the specimen and the grips caused considerable corrosion to occur. They also suggested that the same mechanism might be the reason for similar corrosion observed in ball bearings and between hubs and shafts. Since then numerous cases of fretting damage have been reported.

A common location where fretting can cause fatigue failure is in press fit assemblies of gears and hubs on shafts where bending loads can cause relative cyclic deformation as the shaft rotates [2].

It has also been suggested [3] that fretting is a contributory cause of corrosion in body seams of automobile frames where relative movement occurs in the spot welded joints. The problem is often observed in fabricated structures and, if propagating fatigue cracks are initiated due to fretting, the fatigue strength may be reduced by more than 50 percent [4].

1.2 Subdivision of Fretting Research

From an engineering standpoint fretting can cause failure of a structure by either excessive wear or by the initiation of fatigue cracks. In this context research in fretting is usually subdivided into these two aspects and they are distinguished as two different effects viz:

a. Fretting corrosion

b. Fretting fatigue

2. REVIEW OF CURRENT CONCEPTS IN FRETTING FATIGUE

In the last twenty years considerable effort has been expended on research into fretting fatigue, much of this is reviewed by Waterhouse [5] and Yeh and Sinclair [6]. In this section no attempt will be made to consider all factors which influence fretting fatigue behavior, instead the contents will be restricted to concepts which are significant to subsequent chapters.

2.1 Theories of Fretting Fatigue Crack Initiation

Two theories of crack initiation have been suggested which are consistant with the observed behavior and these are summarized as follows.

2.1.1 Asperity Contact Theory

This was first proposed by Liu, Corten and Sinclair [7] and recently reconsidered by Yeh [8]. The contact between the fretting surfaces is studied at the microscopic level and the asperities which actually touch are considered.

The earlier work analyzed the stress distribution at an asperity and assumed that the contact stress during fretting was sufficient to cause local yielding of the material (Fig. 1). The suggestion was that the fatigue cracks were initiated by these stresses. A summary of this analysis is given in Appendix A.

Yeh's work extends these concepts by considering the contacting points to form cold welded joints. The analysis uses fracture mechanics concepts, and treats the spaces between the joints as small cracks subjected to Mode 2 loading.

2.1.2 Contact Stress Distribution Theory

This was proposed by Nishioku and Hirakawa [9] and also considered by Warton and Waterhouse [10] and Endo, Goto and Nakamura [11].

When two elastic bodies are pressed together a stress distribution is set up over the contact area. This distribution is in general non-uniform and depends on the

geometry of the contacting surfaces. During fretting, shear stresses are superimposed on these static stresses. In the work cited, the magnitude and distribution of the shear stresses are assumed to be given by the product of the coefficient of friction and the normal stress distribution.

The theory postulates that the fatigue cracks are initiated by the maximum cyclic shear stress component associated with these stress distributions. Further details of the analysis is given in Appendix B.

It is seen from Sections 2.1.1 and 2.1.2 that the essential difference between the two theories is a matter of scale--the former looks at microscopic stresses whereas the latter looks at macroscopic effects.

2.2 Factors Influencing Fretting Fatigue

The principal variables effecting fretting fatigue are discussed in the reviews [5] and [6] cited earlier.

In the context of the present work the following results are significant.

2.2.1 Amplitude of Relative Displacement

Fenner and Field [12] and Nishioka and Hirakawa [13] found that the maximum reduction in fatigue strength occurred when the relative slip was of the order of 15 microns (1 micron = 10^{-6} m).

2.2.2 Clamping Pressure

For a given material and contact geometry Corten [14], Liu et al. [7] and Nishioka and Hirakawa [15] all found that fretting fatigue strength decreased rapidly with increasing contact pressure up to a certain value. Further increases above this value resulted in little additional reduction in fatigue strength.

Nishioka and Hirakawa however, found that at the higher values of contact pressure non-propagating cracks were initiated at values of alternating stress below the fretting fatigue strength (Fig. 2).

3. SCOPE AND PURPOSE OF THIS WORK

The research reported in this thesis is restricted to fretting fatigue as defined in Section 1.2. No consideration is given to the fretting corrosion and associated wear which occurred. All the experimental work involved tests in which the fretting was applied simultaneously with the cyclic loading. Assessment of damage was made on the basis of reduction of fatigue strength due to fretting.

The primary objective of the investigation is to assess the "contact stress distribution" theory discussed in Section 2.1.2. Two different fretting geometries which give rise to different contact stress distributions are investigated. These are referred to as cylindrical contact and rectangular contact and are defined in Fig. 3. The work is subdivided into:

a. Consideration of the stress distribution associated with the two geometries, including a review of analytical treatment of the problem and the description of a photoelastic investigation which was carried out to compare the stress distributions experimentally.

b. Description of the experimental work conducted to determine the effect of the two geometries on the fretting fatigue life.

The results of these two aspects of the work are then correlated in an attempt to determine the validity of the theory.

4. MACROSCOPIC STRESSES ASSOCIATED WITH FRETTING CONTACT

Application of the theory of fretting, outlined in Section 2.1.2, to the cases of rectangular and cylindrical contact defined in Section 3.1 necessitates a knowledge of the macroscopic contact stress distribution. This chapter deals with the problem of determining these stresses; the discussion is limited to elastic stresses only, the question of local yielding is considered later in Chapter 6.

4.1 Analytical Treatment

The analysis of the local stresses which are set up, when two bodies are in contact under load, has received considerable attention from elasticians. However, the exact solution of the general case has not been obtained and most of the work is based on various simplifying assumptions. This discussion is limited to the special cases of rectangular and cylindrical contact; for an introduction to the literature on more complex geometric configurations reference should be made to Lubkin [16].

4.1.1 Cylindrical Contact under Normal Force Only

The general plane strain solution for contact between an elastic circular cylinder and an elastic half-plane has not been determined.

The case where the surfaces are frictionless was solved by Hertz [17]. The normal pressure on the contact surface is given by

$$p = \frac{\pi}{4} p_{av} \sqrt{1 - \left(\frac{x}{L}\right)^2} \qquad (4.1)$$

In the present context this is a useful result because it is found that, if the elastic constants are the same for both the cylinder and the plane, then this stress distribution also applies to the case of finite friction.

In the more general case of contact between dissimilar materials with finite friction, tangential stresses are set up along the contact area. This problem has been

considered by Galin [18], Goodman [19] and Spence [20]. Using arguments based on the fully adhesive solution they suggest that slip will occur where

$$\tau > \mu \cdot p \tag{4.2}$$

This defines two parts of the contact area--a central region length "2c" over which no relative movement occurs and the remaining outside region where slip occurs. Results determined by Spence [20] for the case of a rigid cylinder are shown in Fig. 4. It is seen that, for contact between metals where typical values of μ are $\sim .6$, this can result in significant shear stresses. Consequently, the subsequent work, which is limited to contact between similar materials, should be reconsidered for cases of dissimilar materials.

4.1.2 Rectangular Contact under Normal Force Only

The case of an elastic rectangular pad contacting an elastic half plane has not been solved analytically. The only problems which have been solved assume a rigid pad or punch.

The plane strain solution for a rigid pad in the absence of friction was given by Sadowsky [21]. The expression for the normal stress distribution is

$$p = \frac{2p_{av}}{\pi\sqrt{1 - (\frac{x}{L})^2}} \tag{4.3}$$

and is seen to involve a square root singularity of $x = L$.

The case of a rigid pad with fully adhesive contact and with finite friction has been considered by Spence [22] who shows that both shear stress and normal stress acting on the interface become unbounded near the edge of the contact area (Fig. 6).

4.1.3 Contact under Fretting Conditions

The stress distributions, resulting from contact under normal forces only, will be modified if a tangential force is superimposed.

In practice the geometric configuration in fretting situations is usually one in which the control variable is the amplitude of the relative movement. Several investigators have considered the problem of how much relative movement can occur by elastic and plastic deformation without slip occurring over the whole surface. This problem is reviewed by Johnson [23]. The conclusion is that, if the relative displacement exceeds ~ 2.5 microns for steel surfaces, general slip will occur. The experimental work discussed in Chapter 5 involves relative displacements of 25 microns. Consequently, it follows that general slip takes place.

In order to determine the interface shear stress under these conditions it is assumed that a state of Coulomb friction exists so that

$$\tau = \mu p \tag{4.4}$$

If the values of σ and τ on the boundary are known then the stress distribution within the half plane can be determined. One method involves integrating the expressions for a concentrated force on a boundary determined by Mitchell [24] (see also Timoshenko and Goodier [25]).

4.1.4 Cylindrical Contact with Normal and Tangential Forces

This approach has been used by Smith and Liu [26] to determine the stresses associated with cylindrical contact of similar materials. The boundary loading is taken from Eqs. 4.1 and 4.4.

In the notation of Fig. 3 this analysis gave the following results

On the boundary ($y = 0$)

$$\sigma_{xx} = -\frac{4\mu p_{av}}{\pi}\left[\frac{x}{L} - \sqrt{\left(\frac{x}{L}\right)^2 - 1}\right} \qquad x \geq L$$

$$\sigma_{xx} = -\frac{2p_{av}}{\pi}\left[\sqrt{1 - \left(\frac{x}{L}\right)^2} + 2\mu\frac{x}{L}\right] \qquad |x| \leq L \qquad (4.5a)$$

$$\sigma_{xx} = -\frac{4\mu p_{av}}{\pi}\left[\frac{x}{L} + \sqrt{\left(\frac{x}{L}\right)^2 - 1}\right] \qquad x \leq L$$

$$\sigma_{yy} = -\frac{2p_{av}}{\pi}\sqrt{1 - \left(\frac{x}{L}\right)^2} \qquad |x| \leq L$$

$$\sigma_{yy} = 0 \qquad x \geq L \text{ and } x \leq -L \qquad (4.5b)$$

$$\tau_{xy} = -\frac{2\mu p_{av}}{\pi}\sqrt{1 - \left(\frac{x}{L}\right)^2} \qquad |x| \leq L$$

$$\tau_{xy} = 0 \qquad x \geq L \text{ and } x \leq -L \qquad (4.5c)$$

Exact solutions for the stresses at a general point (x, y) were also determined, these expressions have been used to calculate the distribution of maximum shear stress for $\mu = .33$ (Fig. 7).

4.1.5 Rectangular Contact with Normal and Tangential Forces

If the normal stress distribution associated with the elastic rectangular contact were available, the procedure described above could be used to determine the internal stress distribution. The Sadowsky result (Eq. 4.3) could be used but results near the end of contact area ($x \longrightarrow L$) would probably be inexact because of the assumption of a rigid punch. As this is the critical region in fretting fatigue crack initiation, it appears unlikely that this approach would be useful. Consequently, it was decided to carry out a photoelastic analysis of the stress distribution. This is described in the following section.

4.2 Photoelastic Analysis

An experimental investigation was carried out using transmission photoelasticity to determine the stress distribution for both cylindrical and rectangular contact. The details of this work are given in Appendix C.

4.2.1 Summary of Photoelastic Results

It was found that the stress distribution associated with the two geometrical contact configurations differed markedly. Particular attention was given to the material at the edge of the contact area where fretting fatigue cracks usually initiate [27].

The shear stress variation ($\Delta\tau$) which results from reversing the tangential force is discussed in Appendix C, Section C.7.1. The magnitude of $\Delta\tau$ for the two geometries, with $\mu = .33$, was found to be:

	$\Delta\tau$	
	$\frac{y}{L} = .033$	$\frac{y}{L} = .1$
Cylindrical	$.15\ p_{av}$	$.3\ p_{av}$
Rectangular	$>.6\ p_{av}$	$.6\ p_{av}$

at $\frac{x}{L} = 1$.

5. FRETTING FATIGUE BEHAVIOR

5.1 Experimental Program

The fretting tests were carried out using plain carbon SAE 1045 steel for specimen and pad. Material from the same heat had previously been used by Landgraf [28] in work on the fatigue behavior of hardened steels.

Three series of tests were conducted:

a. Standard fatigue tests for baseline data,

b. Fretting fatigue using rectangular pads,

c. Fretting fatigue using cylindrical pads.

5.2 Description of Test Apparatus

5.2.1 Fatigue Machine

All testing was carried out on a MTS 811 axial servo-hydraulic closed loop system. The load control mode was employed, as all tests were carried out at nominally elastic stress levels.

Compression grips were used to reduce risk of failure in the threaded section which had occurred in earlier tests. Axial alignment of the specimen was achieved using a Wood's metal pot [29]. The test system is shown in Fig. 8.

5.2.2 Fretting Configuration

The rig used for the fretting fatigue tests is shown in Figs. 9 and 10. Two fretting shoes (Item 1) were arranged diametrically opposite to each other on the flat surfaces of the specimen. These were loaded normally with the loading ring (Item 4).

During cyclic loading the strain in the specimen causes relative movement at the contact points. The geometry of the pad is such that it is essentially rigid under the loads to which it is subjected, hence the relative movement can be determined from the strain in the specimen and the distance between contacts. Pads were machined with a range of gauge lengths, and for each test the applied cyclic strain and the gauge length of the pads were matched to ensure that the relative slip $\sim$25 microns.

5.2.3 Specimens

Test specimens with the dimensions shown in Figs. 11 and 12 were used for the standard fatigue and fretting fatigue tests respectively. SAE 1045 plain carbon steel, Q & T to 35 R_c hardness, was used; the chemical composition, heat treatment, and mechanical properties are given in Table 1.

5.2.4 Fretting Pads

Details of the rectangular and cylindrical pads are shown in Figs. 13 and 14. These were machined from the same SAE 1045 steel, Q & T to 55 R_c hardness, the mechanical properties are given in Table 1.

5.2.5 Loading Ring

The normal load on the fretting pads was applied with a beryllium-copper loading ring (Item 4, Fig. 9), which was instrumented with electrical resistance strain gauges (Micro-Measurements type MM-EA-06-250BG-120). The ring was used in conjunction with a Baldwin strainmeter type 1200-B. Calibration was carried out using dead weights. The design was such that the ring was sufficiently flexible to ensure that wear at the fretting surface did not result in variation of the normal force applied to the pad.

5.3 Test Results

5.3.1 Rectangular Contact

All tests were carried out under a normal force of 18 lb applied to each pad which is equivalent to a nominal average contact pressure of 3 ksi. Constant amplitude sinusoidal loading was applied to each specimen with zero mean stress. Ten tests were carried out over a range from ± 40 ksi to ± 75 ksi. The results are given in Table 2 and shown graphically in Fig. 15.

5.3.2 Cylindrical Contact

The cylindrical geometry results in some difficulty in defining the contact pressure. The method used was to set up the tests on the basis of the initial average pressure given by normal force ÷ Hertzian contact area. For a steel cylinder 0.6 in. radius on a flat steel surface, the relationship between normal force and average pressure are shown in Fig. 17.

Three different values of average contact pressure were used: 45.4 ksi, 31.9 ksi, 23.1 ksi; five tests were carried out at each pressure.

5.3.3 Standard Fatigue Tests

Some fatigue data had already been determined by Landgraf [28] using the same material and specimen geometry. In order to augment this data, tests were carried out in the region ±80 to ±100 ksi. These results along with those previously determined are given in Table 4 and shown graphically in Fig. 16.

6. ANALYSIS AND DISCUSSION

In the following section the results of the fretting fatigue experiments are first compared with analytical values predicted by the two theories described in Section 2. It is found that neither theory is compatible with the experimental observations.

The process by which the fretting fatigue crack is propagated is then reconsidered with reference to the current experimental results.

6.1 Comparison Between Theoretical Predictions and Experimental Results

The analytical treatments of the asperity and contact stress theories, given in Appendix A and B respectively, both derive equations for predicting fretting fatigue limit.

6.1.1 Asperity Contact Theory

Equation A.6 gives a relationship between fretted and unfretted fatigue strength:

$$\frac{\Delta S_{fN}}{2} = \sqrt{\left(\frac{\Delta S_N}{2}\right)^2 - \frac{\mu^2 \sigma_y^2}{.0378 + \mu^2}}$$

It is seen that this equation takes no account of contact geometry or normal pressure. The experimental results, however, show that the cylindrical contact required an average contact pressure of >23.1 ksi to produce fretting fatigue failure compared with 3 ksi for the rectangular contact.

Substitution of numerical values into the above equation: $\frac{\Delta S_N}{2} = 88$ ksi, $\sigma_y' = 185$, $\mu = .6$ in fact results in an imaginary solution.

6.1.2 Contact Stress Theory

Equation B.10 can be used to predict fretting fatigue strength for cylindrical contact:

$$\frac{\Delta S_{fN}}{2} = \frac{\Delta S_N}{2} - \frac{8}{\pi} p_{av} \mu$$

This equation suggests that increasing the average pressure will reduce the fretting fatigue. The experimental results, however, show that increasing p_{av} above 32 ksi did not effect the fretting fatigue strength.

6.2 Discussion of the Propagation of Fretting Fatigue Cracks

The process by which fretting fatigue failure occurs can be subdivided into two stages:

(i) Crack initiation and growth under the local contact stresses, and

(ii) Crack growth under the cyclically applied loading in material distant from the contact stresses.

An insight into Stage (i) can be gained by first considering Stage (ii). In Section 5.2.1 the concept of a threshold value ΔK is used to define the minimum crack size which will propagate. In Section 6.2.2 fatigue crack propagation equations are used to determine the fraction of the total life which is spent in this stage.

6.2.1 Threshold Crack Size

Work on fatigue crack growth suggests that propagation of a crack will not occur unless the cyclic variation of the stress intensity factor is greater than some threshold value--ΔK_{th} [30]. Experimental results for ΔK_{th} for steels lie between 2 to 4 ksi$\sqrt{in.}$

The stress intensity factor for an edge crack (length a) in a finite member (width B) subjected to axial tension is given by Bowie [31] as:

$$K_1 = \sigma \sqrt{\pi a}\ F(\frac{a}{B}) \qquad (6.1)$$

where $F(\frac{a}{B})$ is given in Fig. 18. For small cracks ($\frac{a}{B} < .10$):

$$F(\frac{a}{B}) = 1.13$$

and the minimum size of crack which will propagate under a given cyclic tensile stress amplitude is obtained from

$$\Delta K_{th} = \frac{\Delta S}{2} \sqrt{\pi a_{th}} \times 1.13 \qquad (6.2)$$

Experimental values of K_{th} are not available for SAE 1045 Q & T to 35 R_c, however Majumdar and Morrow [32] have proposed an equation:

$$\Delta K_{th} = 2(1+n')^{1/2} \sigma_y' \sqrt{\pi \rho^*} \qquad (6.3)$$

where

$$\sigma_y = \sigma_o + \frac{K_y}{\sqrt{\rho^*}} \qquad (6.4)$$

Taking the values suggested by Majumdar and Morrow viz: σ_o = 10.5 ksi and K_y = .564, and other values from [34]; a numerical value of ΔK_{th} may be determined.

However, in the fretting context, the threshold crack size at nominally elastic stresses is probably more likely based on the monotonic yield stress than the cyclic yield stress. With this modification Eq. 6.3 becomes:

$$\Delta K_{th} = 2(1+n')^{1/2} \sigma_y \sqrt{\pi \rho^*} \qquad (6.5)$$

and ΔK_{th} is found to be 2.27 ksi $\sqrt{\text{in.}}$

Using $\frac{\Delta S}{2}$ = 45 ksi as the tensile amplitude at the experimentally determined fretting fatigue limit (Fig. 15) and taking ΔK_{th} = 2.27 ksi $\sqrt{\text{in.}}$; the value of the threshold crack size is found to be

$$a_{th} \sim .001 \text{ in.} \qquad (6.6)$$

It follows from this analysis that surface cracks of the order of .001 in. must be initiated by the Stage (i) fretting process in order to propagate in Stage (ii).

6.2.2 Fatigue Crack Propagation

Majumdar and Morrow [32] have shown that the fatigue crack growth rate can be expressed by:

$$\frac{da}{dN} = \frac{-2(b+c)}{b+c+1}\left[\frac{\sigma_y'}{4(1+n')\,\sigma_f'\,\epsilon_f'}\right]^{\frac{-1}{b+c}}\left\{1-[4(1+n')\,\epsilon_y']^{-\frac{b+c+1}{b+c}}\right\}\frac{\epsilon_y'\,\Delta K^2}{\pi\,\sigma_y'^2} \qquad (6.7)$$

In this expression all the terms other than da/dN and ΔK are properties of the metal considered and hence it has the same form as the empirical equation suggested by Paris, Gomez and Anderson [33]:

$$\frac{da}{dN} = A(\Delta K)^r \qquad (6.8)$$

Using data for SAE 1045 Q & T to 35 R_c from Tucker, Landgraf and Brose [34]

$$A = .79 \times 10^{-7}\ \text{in.}^4/\text{klb} \qquad (6.9)$$

The number of cycles required to extend a crack from a_1 to a_2 is found by integrating 6.8

$$_1N_2 = \int_{a_2}^{a_1} \frac{da}{A(\Delta K)^r} \qquad (6.10)$$

which on substituting for ΔK from 6.1 becomes:

$$_1N_2 \quad \frac{1}{A(\Delta S)^2\,\pi}\int_{a_2}^{a_1} \frac{da}{a\left[F\left(\frac{a}{b}\right)\right]^2} \qquad (6.11)$$

Inspection of the fractured specimens showed that, for $\frac{\Delta S}{2}$ = 50 ksi,[1] the fatigue crack grew to .06 in. before failure. In section 6.2.1 it was shown that a crack of $\sim$.001 in. was initiated in the fretted region.

The number of cycles during which the crack grows from .001 in. to .060 in. therefore represents Stage (ii) of the fretting fatigue process defined in Section 6.1.

Graphical evaluation of Eq. 6.7 gives

$$N_2 = 4.7 \times 10^4 \text{ cycles.}$$

This result shows that crack propagation under the applied cyclic stress occupies $\sim$15 percent of the total life at $\pm$50 ksi. Hoeppner and Goss [35] observed a similar result experimentally:

> "A fretting fatigue damage threshold that results from the fretting was found to exist for both materials. At all load levels a given amount of fretting damage is required before any fatigue life reduction occurs."

The important conclusion from this result is that the development of the crack in the contact stress region occupies 85 percent of the fatigue life, this implies that Stage (i) is essentially a long life fatigue process.[2]

6.3 Discussion of the Initiation of Fretting Fatigue Cracks

The analysis described in Sections 6.2.1 and 6.2.2 suggests that: the fretting process must initiate cracks of the order of .001 in., and that this initiation occupies 2.5 to 3 x 10^5 cycles at a cyclic stress amplitude of 50 ksi.

In this section the initiation of these cracks by the local contact stresses is discussed.

---

[1] Crack growth is assumed to take place during the tensile part of the zero mean stress cycle.

[2] These comments refer to fretting fatigue lives of more than 10^5 cycles which is the region where fretting causes serious reductions in fatigue strength.

6.3.1 Photoelastic Results for the Local Stress Distribution

The results of the photoelastic analysis show that the local cyclic variation of shear stress[3] is significant over depths of $\frac{x}{L} = .1$ for rectangular contact and $\frac{x}{L} = .5$ for cylindrical contact. In the fretting fatigue test geometries this is equivalent to .0015 in. and .0025 in. for the rectangular and cylindrical case respectively.

These depths are consistent with the concept that a .001 in. crack could be initiated by the local stresses.

6.3.2 The Effect of Contact Geometry

The fretting fatigue tests for the two different geometries show two important results:

a. The mean contact pressure necessary to cause fretting fatigue is greater for the case of cylindrical contact than for rectangular contact.

b. The fatigue life behavior is insensitive to contact geometry above certain values of contact pressure.

Conclusion (a) has also been checked with results reported in other research work. Table 5 shows values, taken from the literature, for contact pressures used with the two different geometries. It can be seen that in all cases higher pressures were used with cylindrical contact than for rectangular.

It is suggested that the reason for this difference lies in the magnitude of the local stresses for the two cases. The photoelastic results show that, at a depth equivalent to .001 in., in the fatigue specimen, the rectangular contact results in a local shear stress amplitude which is at least 4 x the magnitude which results from cylindrical contact under the same average pressure.

---

[3] Crack initiation is assumed to occur on the plane of maximum shear stress.

Conclusion (b) is a similar result to that reported in Refs. 7, 14 and 15 where it was observed that, above a certain value, raising the normal pressure does not effect fretting fatigue strength.

It appears possible that the reason for this result involves local plastic flow. The high stress concentration in the rectangular case suggests that under an average pressure of 3 ksi some local yielding occurs at the edge of the contact area. The cylindrical contact is analyzed below using the method of Appendix B.

Equation B.9 gives an expression for the maximum cyclic shear stress amplitude for a given cyclic stress amplitude and average contact pressure:

$$\frac{\Delta\tau}{2} = \frac{\Delta S}{2} + \frac{8}{\pi}\mu\, p_{av}$$

for $\Delta S = 90$ ksi $p_{av} = 23$ ksi and $\mu = .6$

$$\frac{\Delta\tau}{2} = 45 + 35 = 80 \text{ ksi}$$

The value of the tensile yield stress for the material from [34] is 185 ksi and taking the Tresca Yield condition this would require:

$$\frac{\Delta\tau}{2} = 92.5 \text{ ksi for local yielding}$$

Hence it is seen that, for the lowest average contact pressure used during the cylindrical contact fretting tests, yielding does not occur.[4]

At higher normal pressures yielding will occur and the shear stress amplitude will remain constant at the yield value. It is suggested that under these conditions the fretting fatigue life will be independent of geometry.[5]

---

[4] In fact, changes in σ_y will occur because of cyclically dependent softening but these have been ignored here.

[5] The two different geometries do result in different volumes of highly stressed material as indicated by the photoelastic analysis. However, these differences are too small to result in any significant size effect on the fatigue strength.

7. SUMMARY AND CONCLUSIONS

The experimental investigation into the fretting fatigue behavior of SAE 1045 steel Q & T to 35 R_c in contact with a pad of SAE 1045 Q & T to 55 R_c showed the following results:

1. The fretting resulted in a reduction in fatigue strength of ~50 percent.
2. Variation of the contact pad geometry indicated that:
   a. Higher average contact pressures were required to cause fatigue failure with cylindrical pads than with rectangular pads.
   b. Above some limiting value of contact pressure for each geometry, the fretting fatigue-life curve was the same.

Analysis of the experimental data from the fretting fatigue tests and an associated photoelastic study, showed that the local stress magnitudes resulting from the fretting contact were consistent with a fretting fatigue model, which comprises the following stages:

1. Growth of a crack under the local stresses for ~85 percent of the total life.
2. Propagation of that crack by the cyclically applied stress during the remaining 15 percent of the life.

The experimental observations and discussions in Sections 6.2.1 and 6.2.3, suggest that the local stresses are important in the fretting fatigue crack initiation stage at the macroscopic level.

On a microscopic scale, however, it seems likely that the asperity contact stresses will result in the formation of small fatigue cracks as described by Yeh [8].

It is suggested that the two theories of fretting fatigue described in Section 2.1 are both involved in the crack initiation process which comprises:

1. Formation of microscopic cracks by asperity contact.
2. Growth of these cracks under the local macroscopic stresses up to a size which can propagate under the applied cyclic stress.

LIST OF REFERENCES

1. Eden, E. M., Rose, W. N. and Cunningham, F. L., "The Endurance of Metals," Proceedings of Institution of Mechanical Engineers, 4, p. 839, 1911.

2. Peterson, R. E. and Wahl, A. M., "Fatigue of Shafts at Fitted Members with Related Photoelastic Analysis," Journal of Applied Mechanics, Vol. 2, p. A1, 1935.

3. Jacobson, M. A. I., "Fretting Corrosion in Automobile Body Seams," Proceedings of Institution of Mechanical Engineers, 182, p. 134, 1967.

4. Grover, H. J., Gordon, S. A. and Jackson, L. R., "Fatigue of Metals and Structures," U.S. Navy Report 00-25-534, 1960.

5. Waterhouse, R. B., Fretting Corrosion, Pergamon Press, 1972.

6. Yeh, H. C. and Sinclair, G. M., "A Review of Fretting Fatigue," University of Illinois, College of Engineering, Fracture Control Program Report No. 8, 1973.

7. Liu, H.W., Corten, H. T. and Sinclair, G. M., "Fretting-Fatigue Strength of Titanium Alloy R. C. 130 B," American Socicty of Testing and Materials, Vol. 57, p. 623, 1957.

8. Yeh, H. C., "An Analysis of Fretting Damage on Fatigue Strength," Ph. D. Thesis, University of Illinois, College of Engineering, 1974.

9. Nishioka, K. and Hirakawa, K., "Fundamental Investigation of Fretting Fatigue (Part 2. Fretting Fatigue Testing Machine and Some Test Results)," Bulletin of Japanese Society of Mechanical Engineers, Vol. 12, p. 180, 1969.

10. Warton, M. H. and Waterhouse, R. B., "The Effect of Different Contact Materials on the Fretting Fatigue Strength of Aluminum Alloy," Wear, 26, pp. 253-260, 1973.

11. Endo, K., Goto, H. and Nakamura, T., "Fretting Fatigue Strength of Several Materials Combinations," Bulletin of Japanese Society of Mechanical Engineers, Vol. 16, No. 92, p. 143, 1973.

12. Fenner, A. J. and Field, J. E., "La Fatigue dans Pes Conditions de Frottement," Revue de Metallurgie LV, No. 5, p. 475, 1958.

13. Nishioka, K. and Hirakawa, K., "Fundamental Investigations of Fretting Fatigue (Part 5. The Effect of Relative Slip Amplitude)," Bulletin of Japanese Society of Mechanical Engineers, Vol. 12, p. 629, 1969.

14. Corten, H. T., "Factors Influencing Fretting Fatigue Strength," Department of Theoretical and Applied Mechanics, University of Illinois, T. & A.M. Report No. 88, 1955.

15. Nishioka, K. and Hirakawa, K., "Fundamental Investigations of Fretting Fatigue (Part 6. Effects of Contact Pressure and Hardness of Materials)," Bulletin of Japanese Society of Mechanical Engineers, Vol. 15, p. 135, 1972.

16. Lubkin, J. L., Contact Problems--Handbook of Engineering Mechanics, Chapter 42, Editor, Flugge, W., McGraw Hill, 1962.

17. Hertz, H., Miscellaneous Papers, translated by Jones, D. E. and Schott, G., MacMillan, New York, 1896.

18. Galin, L. A., "Contact Problems in Elasticity," English translation by Sneddon, I. N., North Carolina State College, Department of Mathematics and Engineering Research Report.

19. Goodman, L. E., "Contact Stress Analysis of Normally Loaded Rough Spheres," Journal of Applied Mechanics, p. 515, September, 1962.

20. Spence, D. A., "Self Similar Solutions to Adhesive Contact Problems with Incremental Loading," Proceedings of the Royal Society, Series A, 305, pp. 55-80, 1968.

21. Sadowsky, M., "Zweidimensionale Probleme der Elastizitätstheorie," Zeitschrift für Angewandte - Mathematic und Mechanik, Vol. 8, p. 107, 1928.

22. Spence, D. A., "An Eigenvalue Problem for Elastic Contact with Finite Friction," Proceedings of Cambridge Philosophical Society, Vol. 73, p. 249, 1973.

23. Johnson, K. L., "Surface Interactions Between Elastically Loaded Bodies under Tangential Forces," Proceedings of the Royal Society, Series A, 230, p. 531, 1955.

24. Mitchell, J. H., "Elementary Distributions of Plane Stress, Proceedings of the London Mathematical Society, Vol. 32, p. 35, 1900.

25. Timoshenko, S. P. and Goodier, J. N., Theory of Elasticity, McGraw-Hill, Third Edition, 1970.

26. Smith, J. O. and Liu, C. K., "Stress Due to Tangential and Normal Loads on an Elastic Solid with Applications to Some Contact Stress Problems," Journal of Applied Mechanics, p. 157, June, 1973.

27. Waterhouse, R. B. and Taylor, D. E., "The Initiation of Fatigue Cracks in a 0.7% Carbon Steel by Fretting," Wear, Vol. 17, pp. 139-147, 1971.

28. Landgraf, R. W., "Cyclic Deformation and Fatigue Behavior of Hardened Steel, Department of Theoretical and Applied Mechanics, University of Illinois, T. & A. M. Report No. 320, 1968.

29. Feltner, C. E. and Mitchell, M. R., "Basic Research on the Cyclic Deformation and Fracture Behaviour of Materials," Manual on Low Cycle Fatigue Testing, ASTM STP 465, American Society for Testing and Materials, pp. 27-66, 1969.

30. Bucci, R. J., Paris, P. C., Hertzberg, R. W., Schmidt, R. A. and Anderson, A. F., "Stress Analysis and Growth of Cracks," Proceedings of the 1971 National Symposium on Fracture Mechanics, Part I, ASTM STP 513, pp. 125-140, 1972.

31. Bowie, O. L., "Single Edge Crack in a Rectangular Tensile Sheet," Transactions of American Society of Mechanical Engineers, Series E, Journal of Applied Mechanics, Vol. 32, p. 708, 1965.

32. Majumdar, S. and Morrow, JoDean, "Correlation Between Fatigue Crack Propagation and Low Cycle Fatigue Properties," Department of Theoretical and Applied Mechanics, University of Illinois, T. & A. M. Report No. 364, 1973.

33. Paris, P. C., Gomez, M. P. and Anderson, W. E., "A Rational Analytic Theory of Fatigue," The Trend in Engineering, University of Washington, Vol. 13, No. 1, p. 9, 1961.

34. Tucker, L. E., Landgraf, R. W., Brose, W. R., "Proposed Technical Report on Fatigue Properties for the SAE Handbook," SAE Report No. 740279, 1974.

35. Hoeppner, D. W. and Goss, G. L., "A Fretting-Fatigue Damage Threshold Concept," Wear, Vol. 27, pp. 61-70, 1974.

36. Yeh, H. C., Private communication, Department of Theoretical and Applied Mechanics, University of Illinois, 1974.

37. Frocht, M. M., Photoelasticity, John Wiley & Sons, New York, Vol. 1, 1941.

38. Hoeppner, D. W. and Goss, G. L., Lockheed Report 25317, Lockheed-California Company, Burbank, 1972.

39. Collins, J. A. and Tovey, F. M., "The Effect of Fretting Damage on the Fatigue Behavior of Metals, Journal of Materials, Vol. 7, No. 4, pp. 460-464, 1972.

40. Malkin, S., Majors, D. P. and Courtney, T. H., "Surface Effects During Fretting Fatigue of Ti-6Al-4V," Wear, Vol. 22, pp. 235-244, 1972.

41. Prandtl, L., "Über die Eindringungsfestigkeit (Härte) Plastischer Baustoffe und die Festigkeit von Schneiden," Zeitschrift für Angewandte Mathematik und Mechanik, Vol. 1, No. 1, pp. 15-20, 1921.

TABLE 1 CHEMICAL AND MECHANICAL PROPERTIES OF SAE 1045 STEEL

a. Chemistry

Material	C	Si	Mn	S	P	Cr	Mo	Ni	Cu
SAE 1045	0.48	0.20	0.71	0.025	0.014	<0.05	<0.03	<0.05	0.05

b. Processing

Cold drawn to 9/16 in rounds from hot rolled rod.
Austenitized 1500°F (oxidizing atmosphere)/20 minutes, water quenched at 70°F.

c. Mechanical Properties

Material	Treatment	Hardness (R_c)	Modulus of Elasticity ksi	Yield Strength ksi	Ultimate Strength ksi	Reduction in Area %
SAE 1045	Q & T at 720°F	35	30,000	185	195	59
SAE 1045	Q & T at 360°F	55	30,000	270	325	41

TABLE 2 FRETTING FATIGUE RESULTS--RECTANGULAR CONTACT

Force/Shoe (lb)	Mean Contact Pressure p_{av} (ksi)	Stress Amplitude $\frac{\Delta S}{2}$ (ksi)	Number of Cycles to Failure (N_f)	Remarks
18	3	75	165,100	
		60	188,100	
		45	5,025,100	Did not fail
		52.5	307,100	
		49	290,200	
		45	3,018,900	
		37.7	10^7	Did not fail
		40	10^7	Did not fail
		50	450,300	
		50	773,800	

TABLE 3 FRETTING FATIGUE RESULTS--CYLINDRICAL CONTACT

Force/Shoe (lb)	Mean Contact Pressure-p_{av} (ksi)	Stress Amplitude $\frac{\Delta S}{2}$ (ksi)	Number of Cycles to Failure (N_f)	Remarks
72	45.4	60	401,200	
		55	247,500	
		50	162,300	
		50	310,700	
		40	10^7	Did not fail
36	31.9	55	195,200	
		50	898,700	
		47.5	1,859,200	
		47.5	5×10^6	
		55	225,500	Did not fail
18	23.1	55	5×10^6	Did not fail
		60	10^7	Did not fail
		65	5×10^6	Did not fail
		70	2,010,200	
		70	2,853,100	

TABLE 4 FATIGUE RESULTS

Material	Elastic Stress Amplitude $\frac{\Delta S}{2}$ (ksi)	Number of Cycles to Failure	Remarks
SAE 1045	100	41,000	Computed from Ref. 29
(Q & T 720°F)	124	7,500	Computed from Ref. 29
35 R_c	128	3,000	Computed from Ref. 29
	80	3,629,300	Failed in Grips
	90	2,119,400	
	95	301,500	
	87.5	5×10^6	

TABLE 5 CONTACT DATA

Source	Geometry	Material		Average Pressure (ksi)
		Specimen	Pad	
Hoeppner & Goss (Ref. 38)	Rectangular	7075-TS Ti-6Al-4V	7075-TS Ti-6Al-4V	3
Liu et al. (Ref. 7)	Rectangular	R_c 130 B	SAE 4340	15
Waterhouse & Taylor (Ref. 27)	Rectangular	Al. Alloy (British Spec. L. 65)	Al. Alloy (L 65)	9
Collins & Tovey (Ref. 39)	Rectangular	SAE 4340	SAE 4340	10
Nishioka & Hirakawa (Ref. 9)	Cylindrical	.7% C Steel Normalized	.7% C Steel As received	60
Endo et al. (Ref. 11)	Cylindrical	.5% C Steel	.5% C Steel	100
Malkin et al. (Ref. 40)	Cylindrical	Ti-6Al-4V	Ti-4Al-4V	31

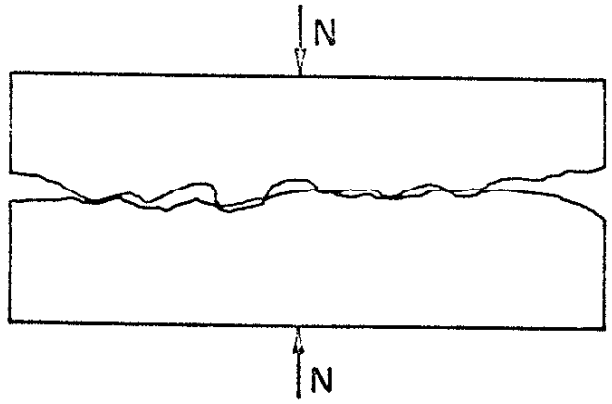

(a)

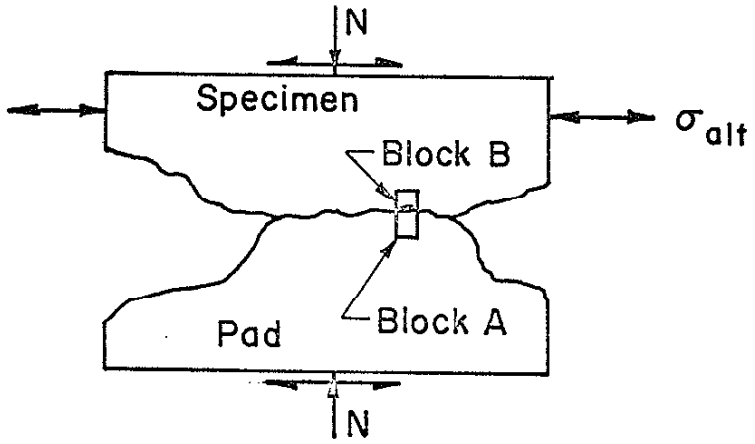

(b)

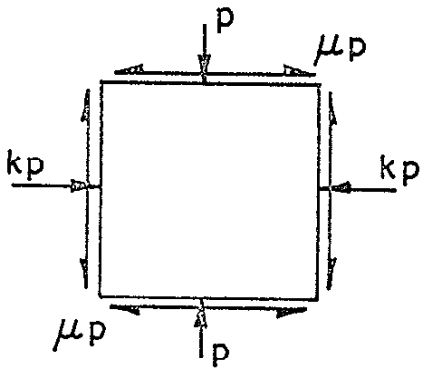

(c) Stress Due to Fretting

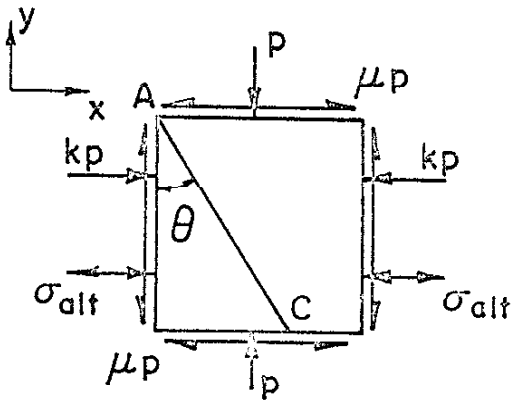

(d) Stress Due to Fretting and Fatigue Loading

Fig. 1 Contacting Asperities and Associated Stress

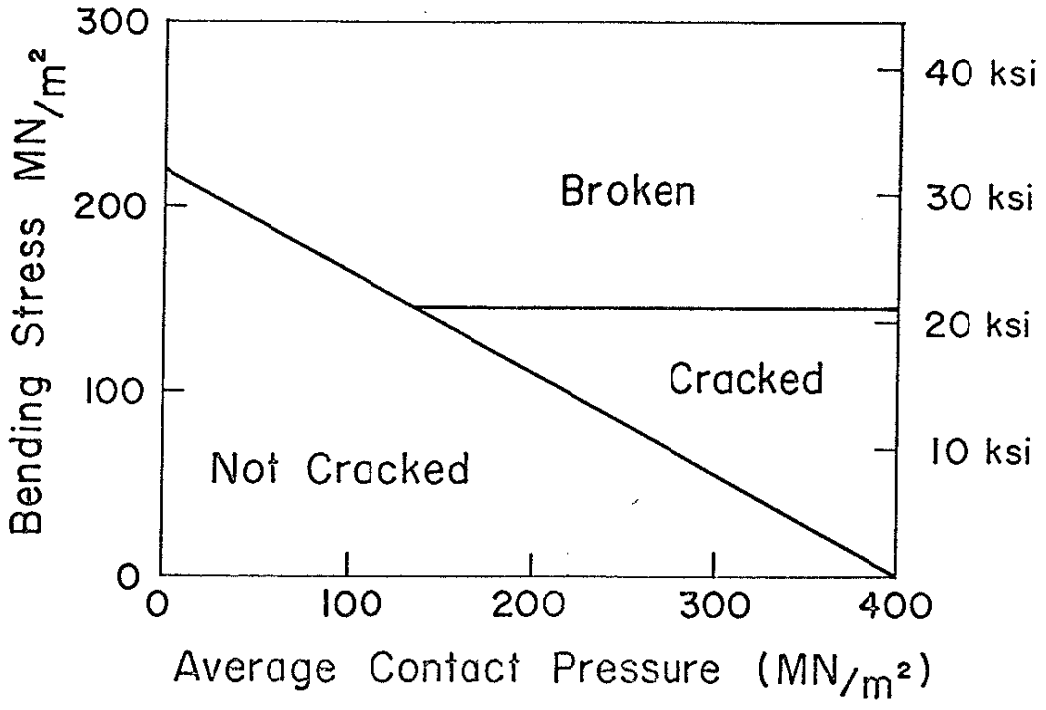

Fig. 2 Effect of Contact Pressure on the Fretting Fatigue Strength (from ref. 16)

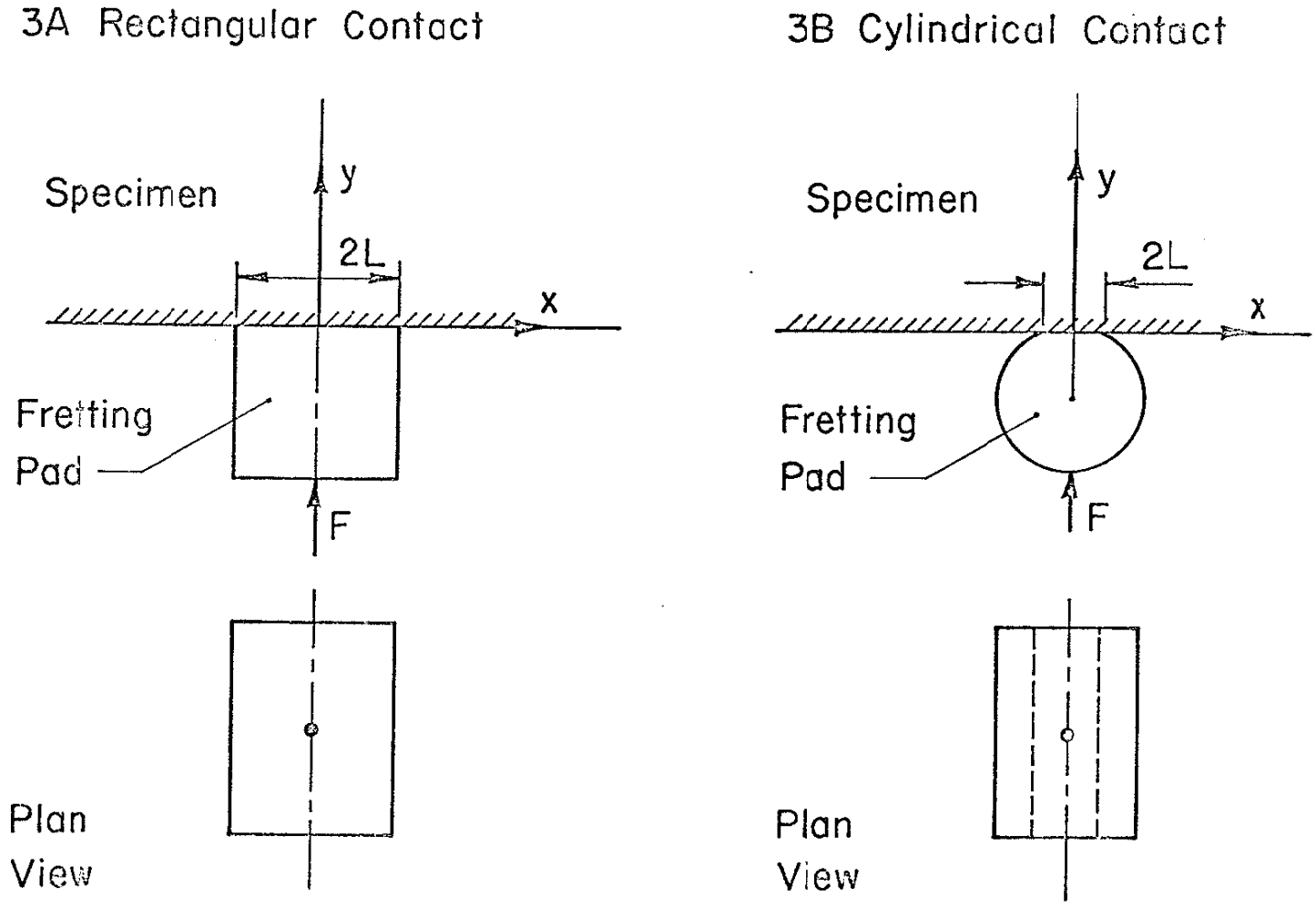

Fig. 3 Contact Geometry

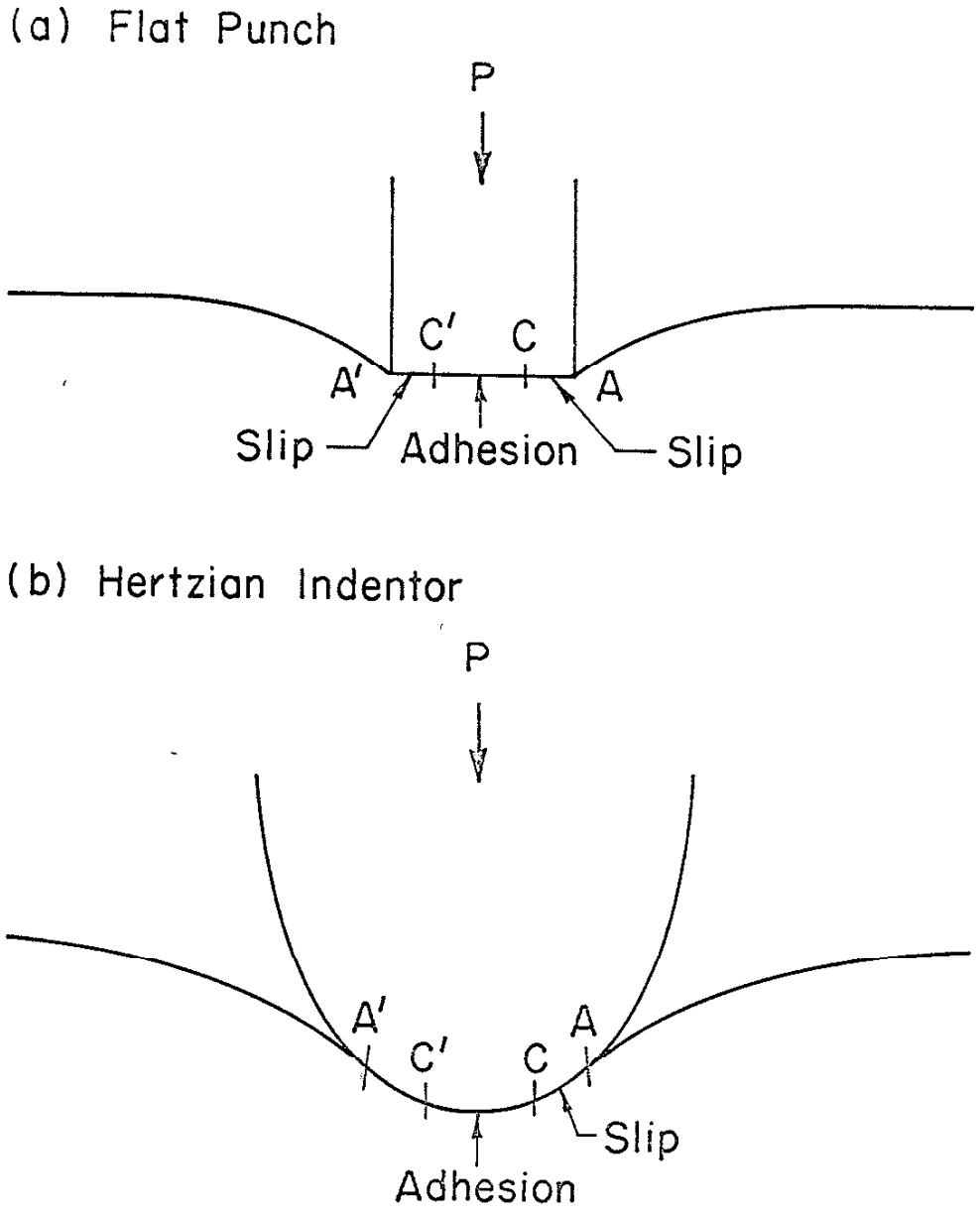

Fig. 4 Frictional Indentation by Rigid Punch (schematic). (from ref. 23)

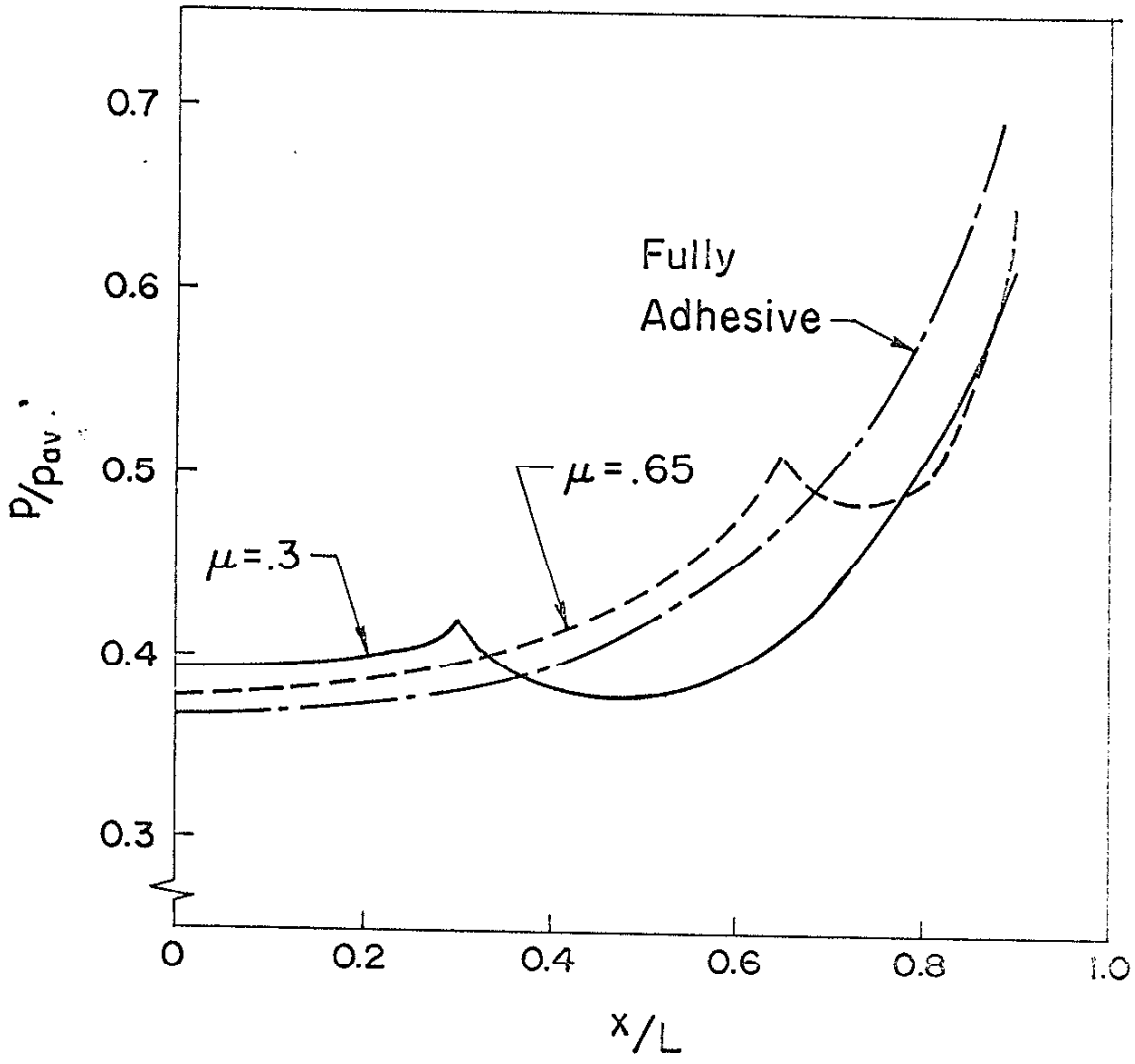

Fig. 5 Normal Pressure Under a Rigid Flat Pad (from ref. 23)

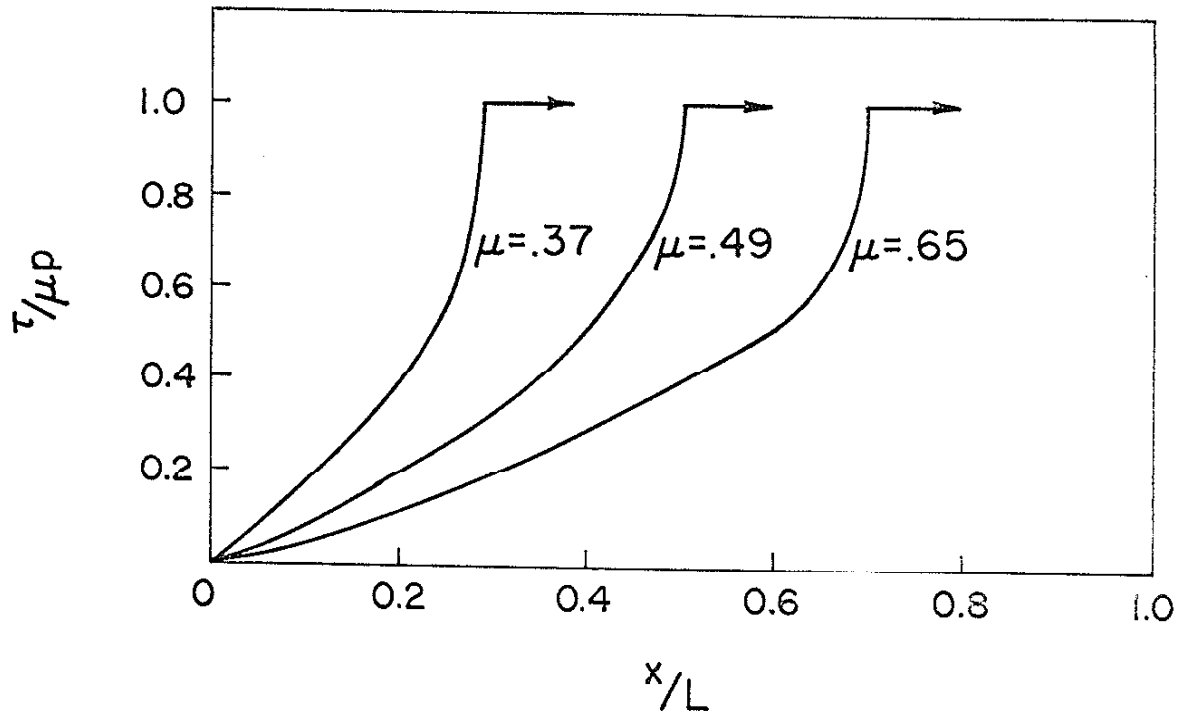

Fig. 6 Shear Stress Distribution for Rigid Flat Pad (from ref. 23)

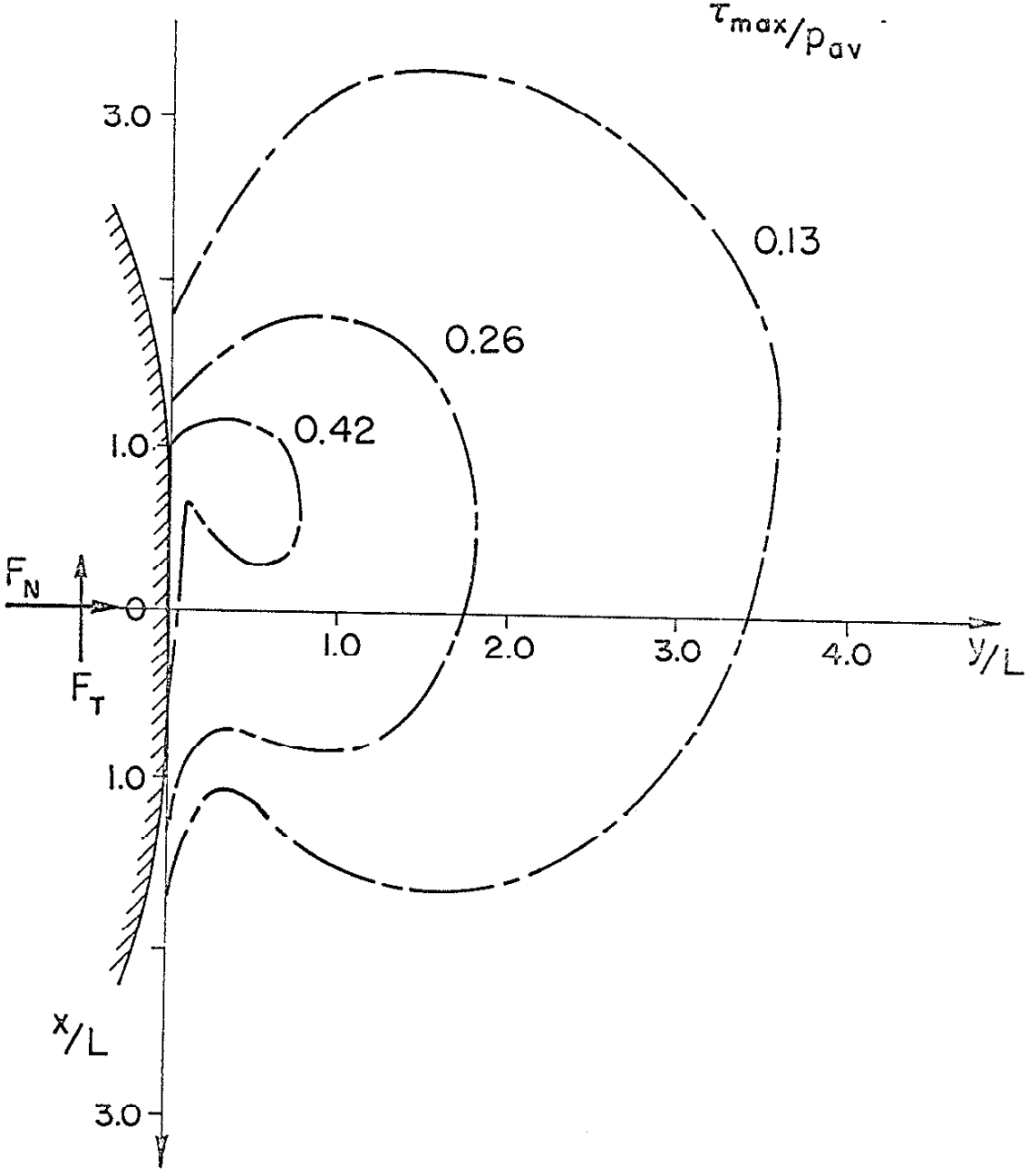

Fig. 7 Analytical Results for Maximum Shear Stress Distribution for Cylindrical Contact $\left[\frac{F_T}{F_N} = \frac{1}{3}\right]$

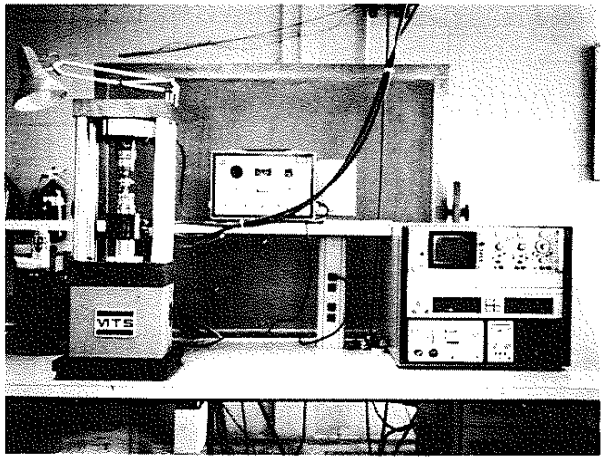

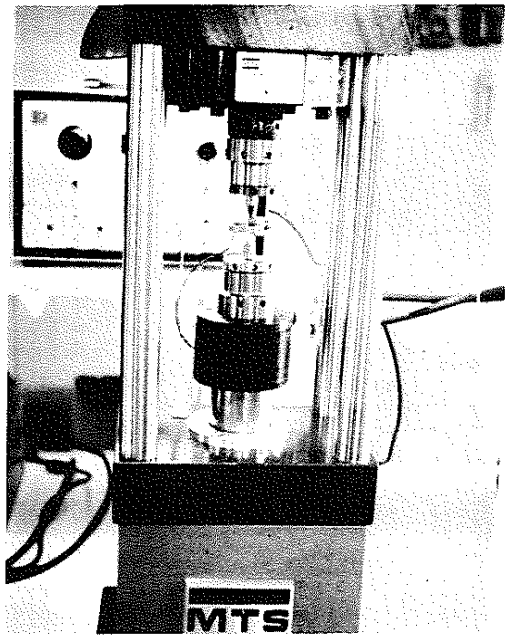

Fig.8 Fatigue Test System

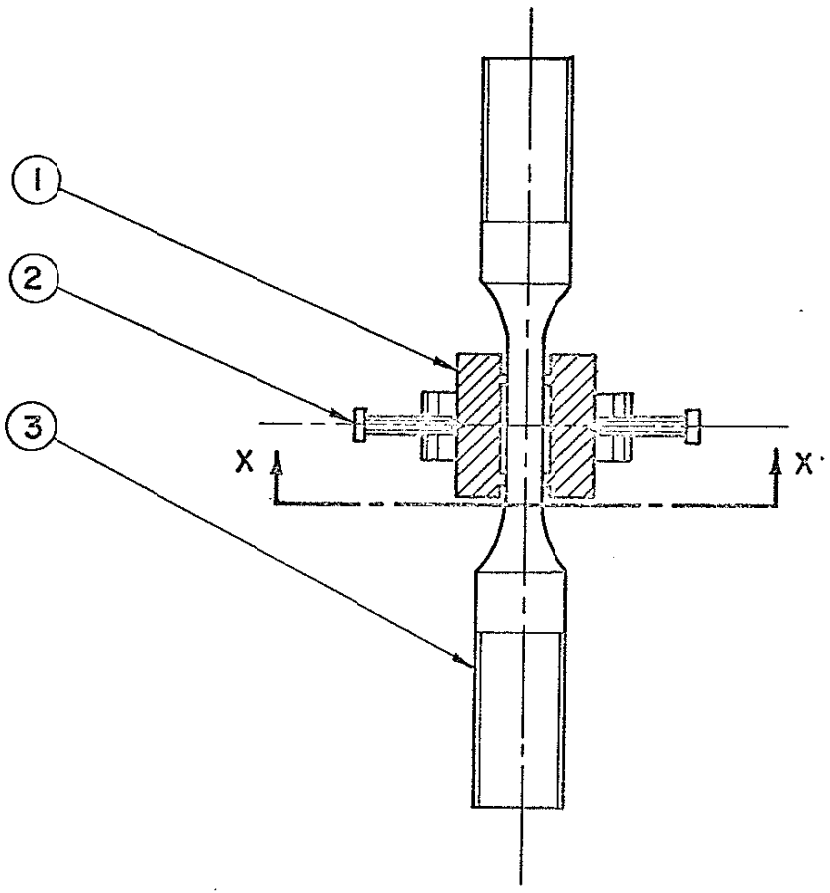

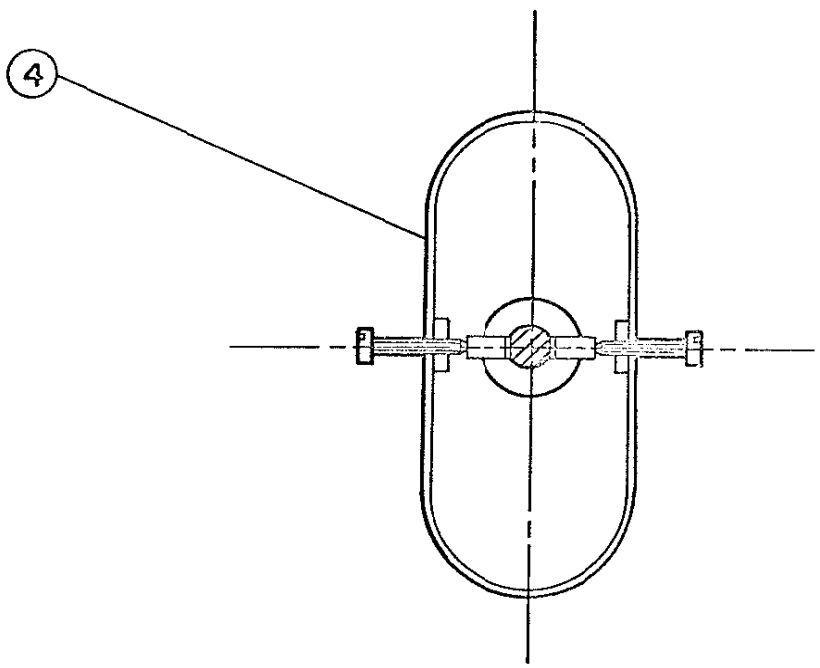

Section on x–x

Scale : ~ full size

ITEM NO.	DESCRIPTION
1	FRETTING SHOE
2	LOAD SCREW
3	SPECIMEN
4	LOADING RING

Fig. 9 Fretting Jig

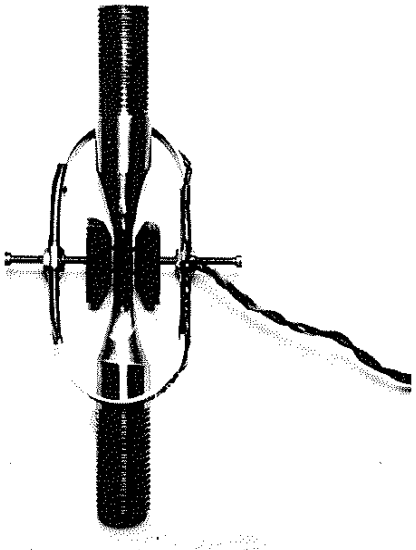

Fig. 10 Fretting Jig

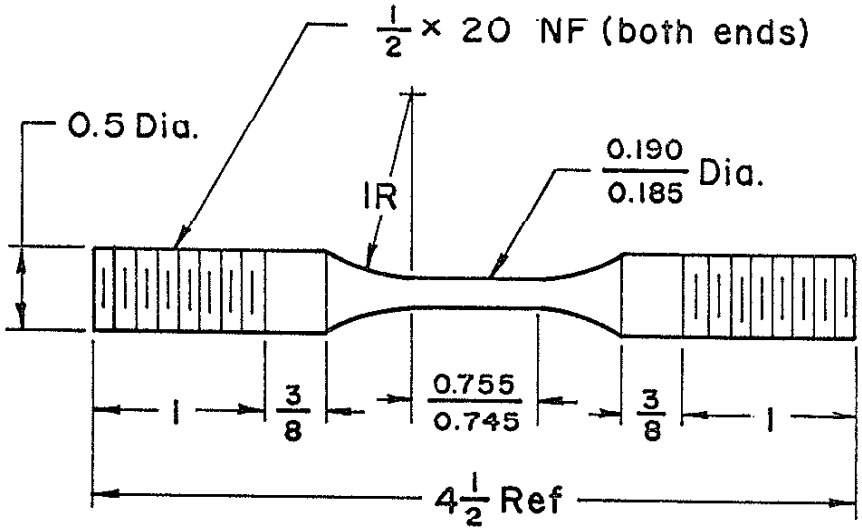

Notes:

1. All dimensions in inches.
2. Fractional dimensions within ± $\frac{1}{32}$ in.
3. Test section diameter uniform to within ± 0.0005 in. along gage length.

Fig. 11 Basic Fatigue Test Specimen

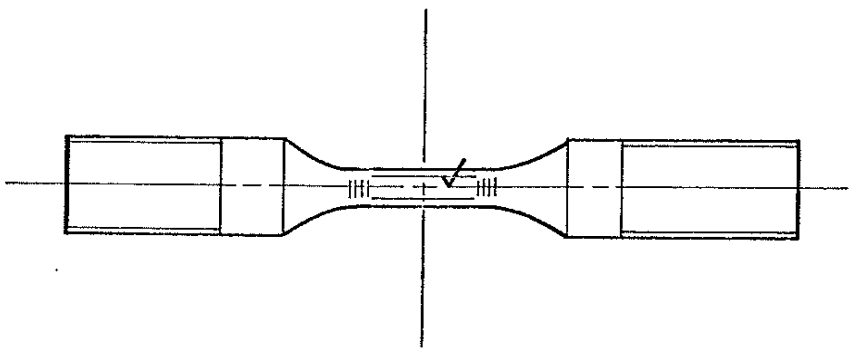

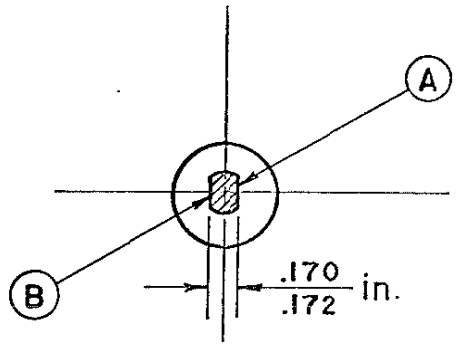

Faces ✓ ground flat
to dimensions shown

Note: Faces (A) and (B) to be ground alternately, removing no more than 0.002 in. from either side at any time.

Fig. 12 Modified Specimen for Fretting

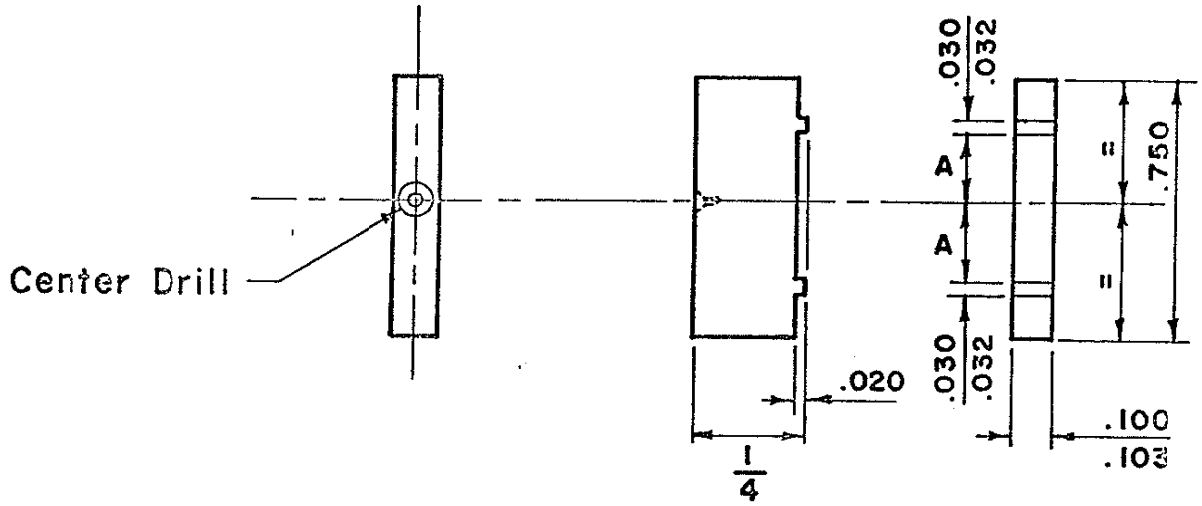

PART No.	DIM. 'A'
1	.010
2	.085
3	.135
4	.185
5	.235
6	.285
7	.335

Fretting Shoe
SAE 1045 (As Quenched)
Scale : 2:1
All Dimensions are in Inches

Fig. 13 Rectangular Fretting Shoe

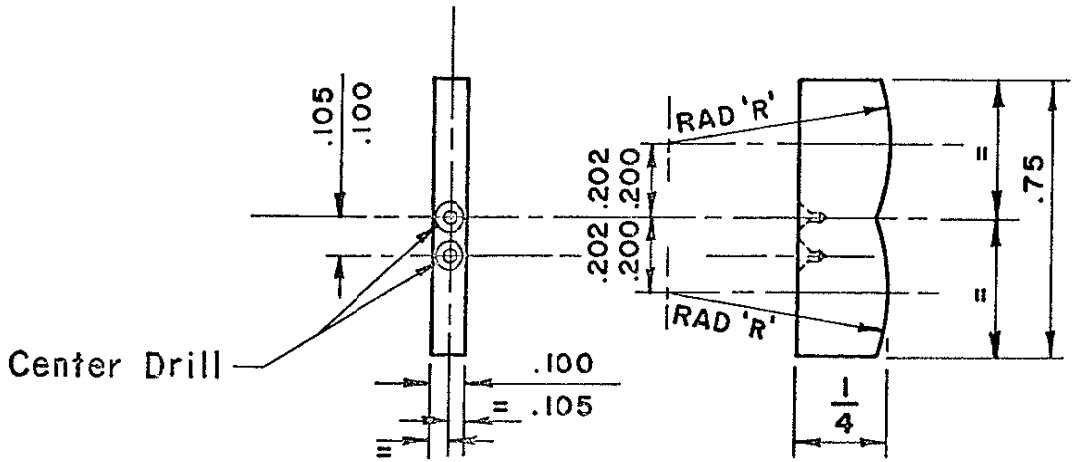

PART No.	RAD 'R'
1	.600
2	2.00

Fretting Shoe
SAE 1045 (As Quenched)
Scale : 2 : 1
All Dimensions are in Inches

Fig. 14 Cylindrical Fretting Shoe

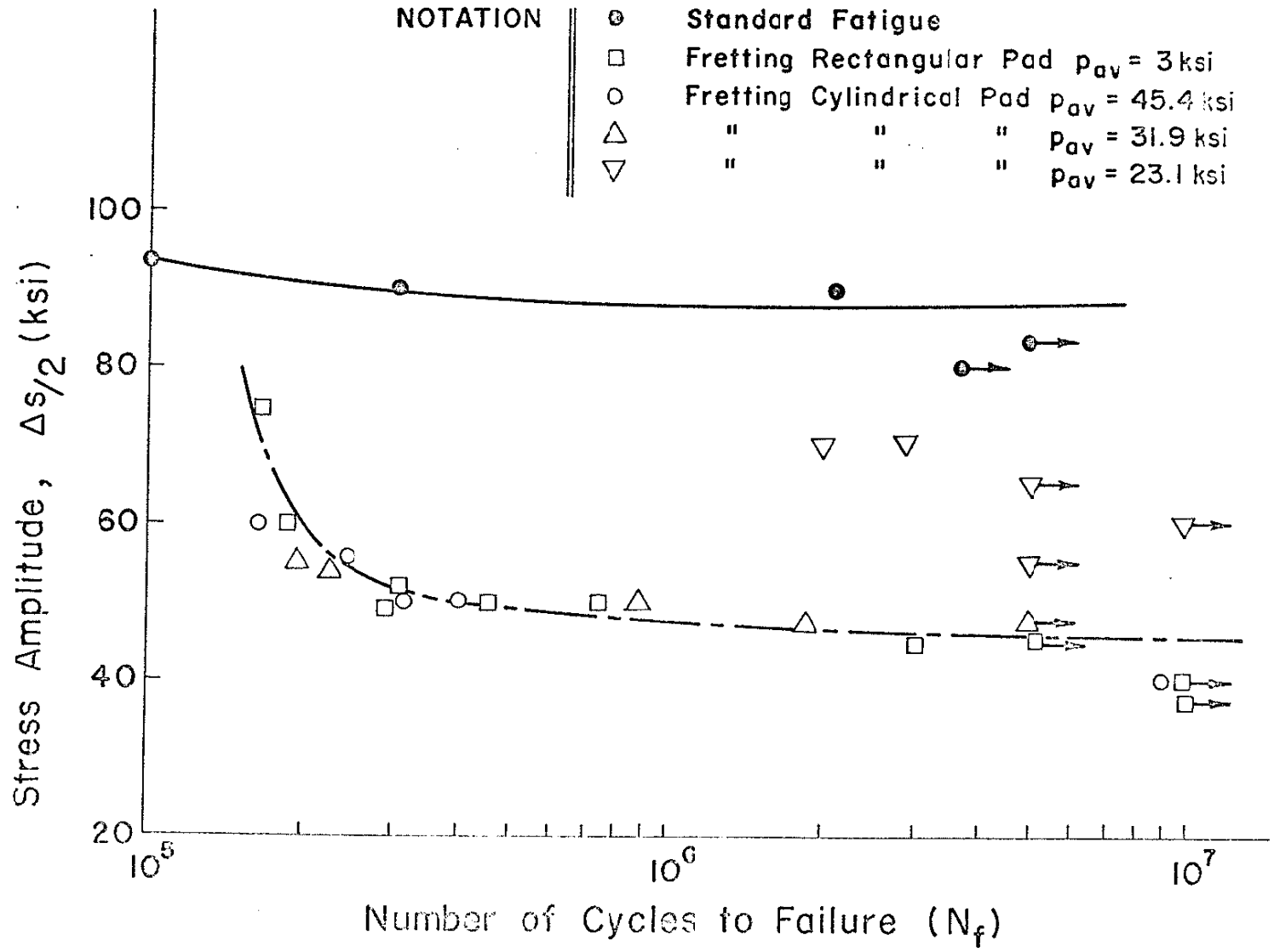

Fig. 15 Fretting Fatigue — Stress-Life Curve

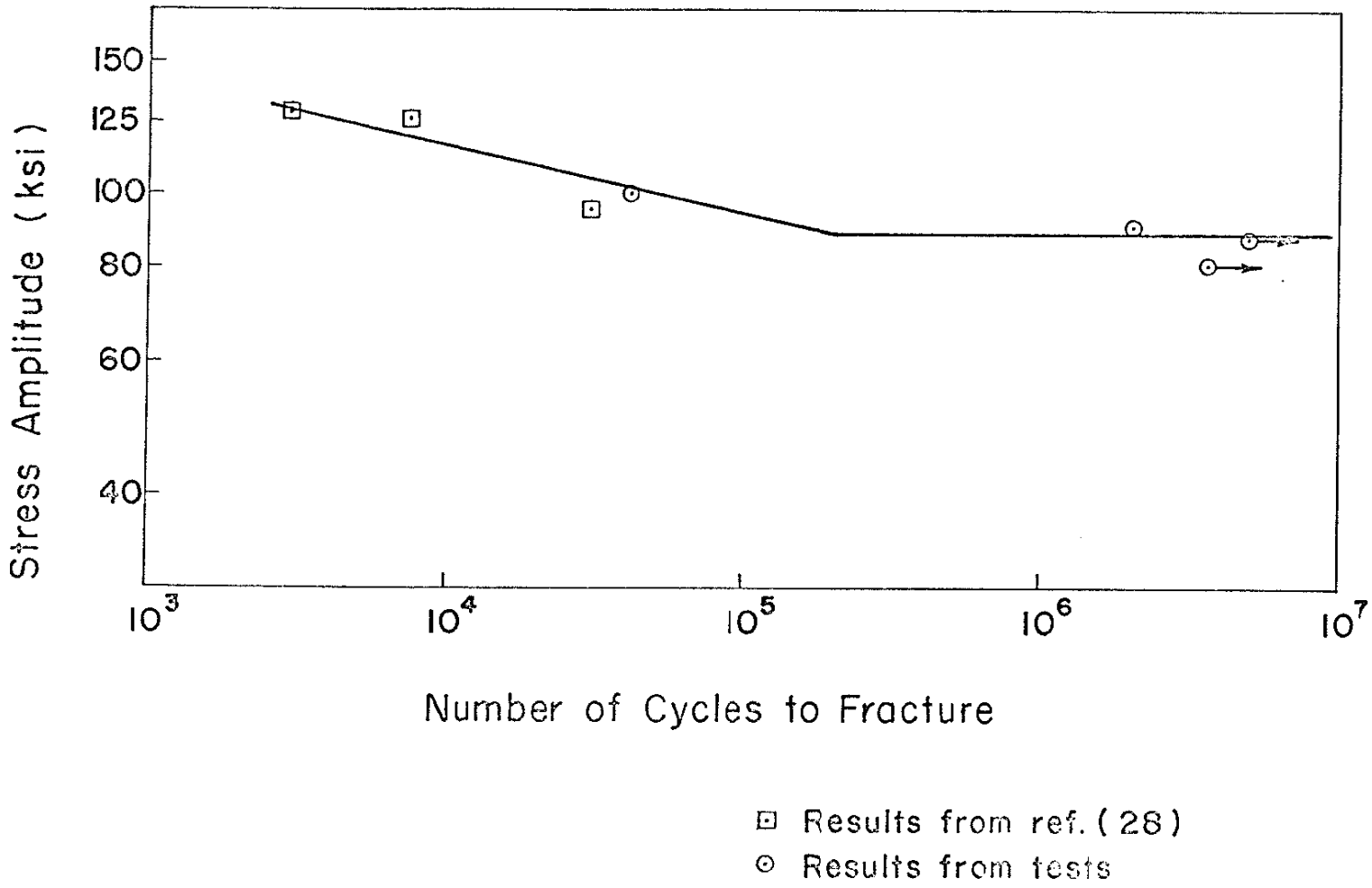

Fig. 16 Standard Fatigue — Stress–Life Curve

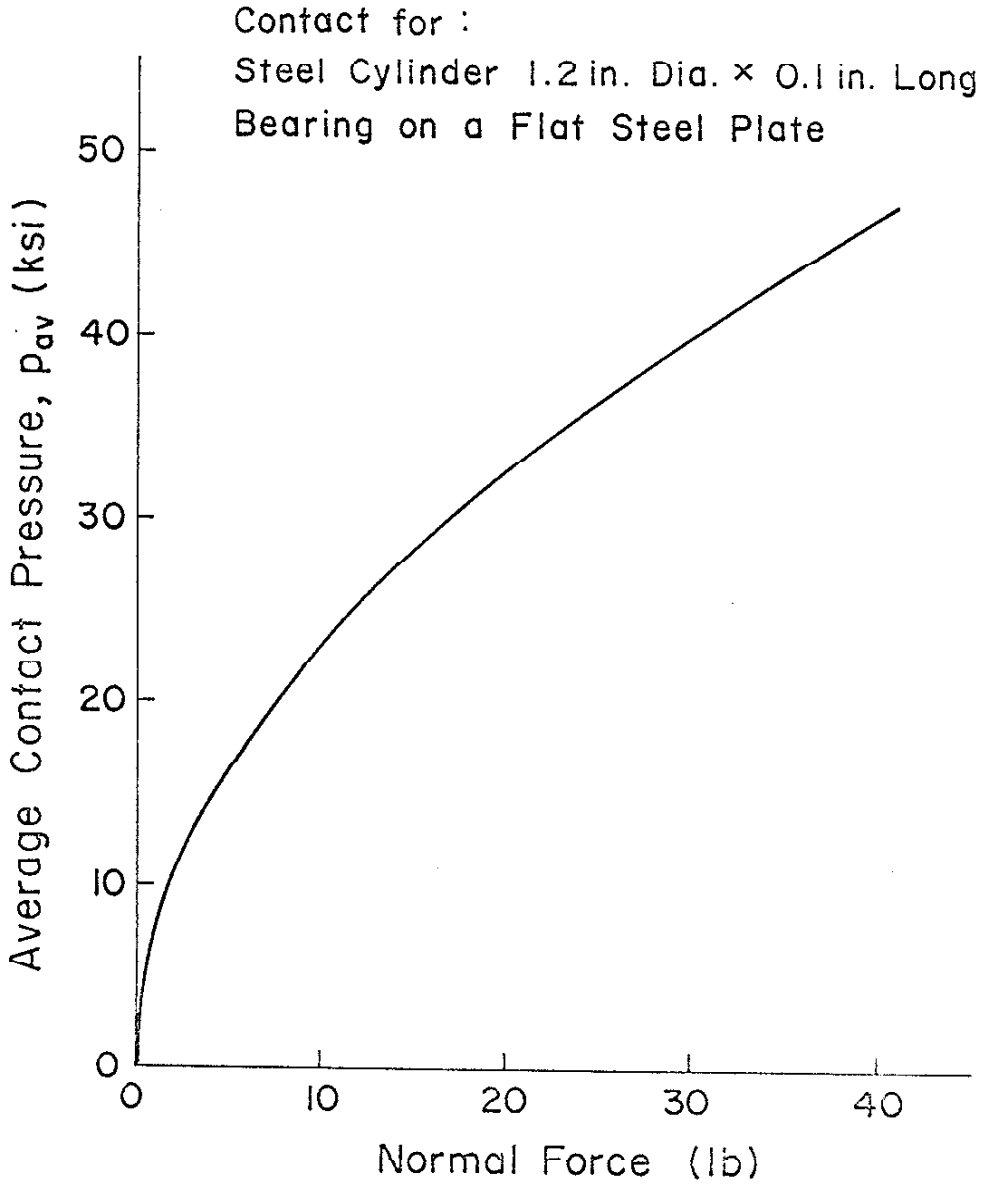

Fig. 17 Average Pressure, Cylindrical Contact

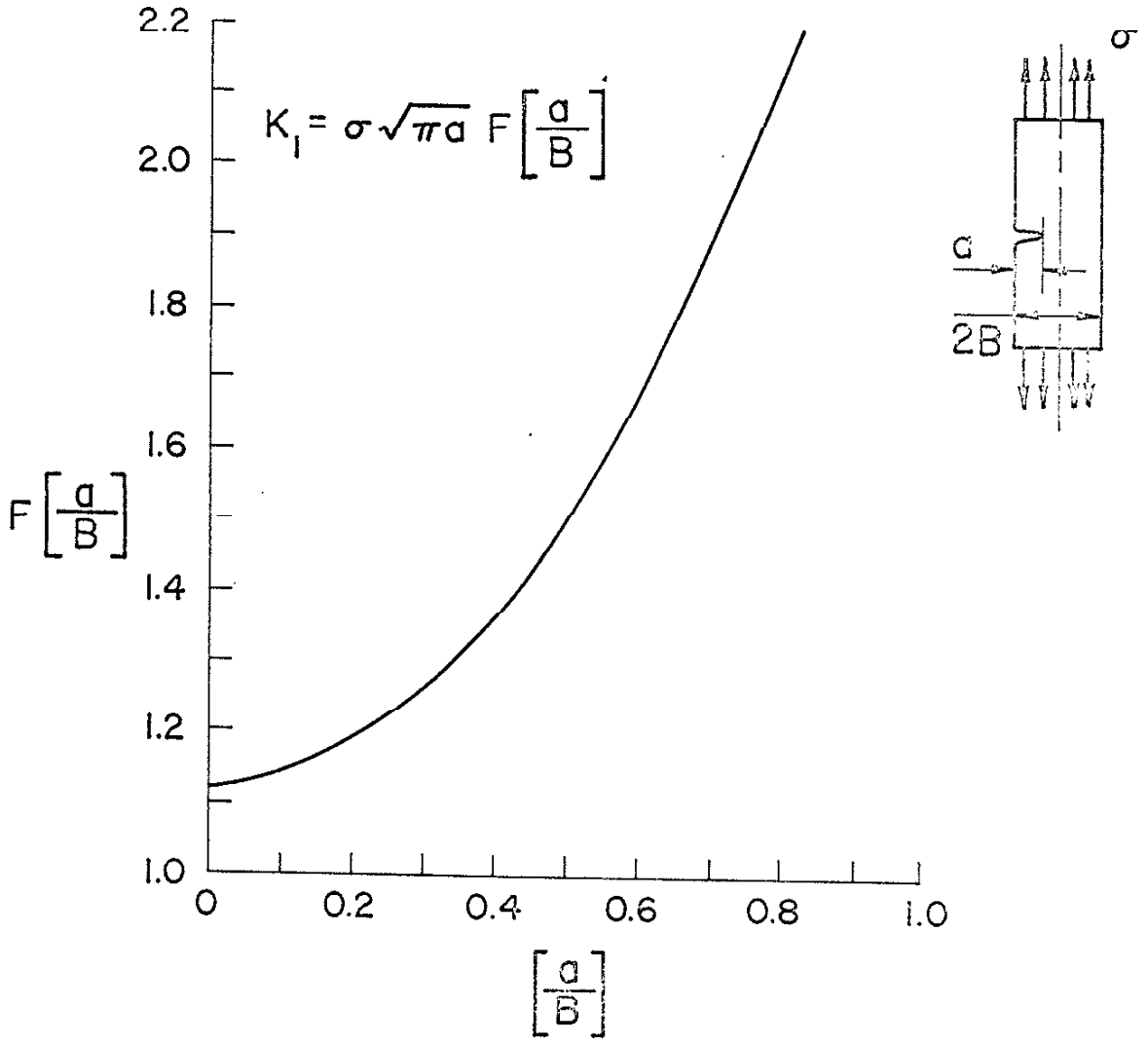

Fig. 18 Stress Intensity Factor (from ref. 31)

APPENDIX A

ANALYSIS OF ASPERITY STRESSES DURING FRETTING FATIGUE

With reference to Fig. 1.

A.1 Contact Pressure

The Normal pressure on the asperities is determined from the contact before the alternating stress is applied, and is given by

$$\tau_{max} = \sqrt{\left(\frac{\sigma_{xx} - \sigma_{yy}}{2}\right)^2 + \tau_{xy}^2}$$

or

$$\tau_{max} = p\sqrt{\left(\frac{k - 1}{2}\right)^2 + \mu^2} \qquad (A.1)$$

This stress will cause yielding in the asperities of the pad or the specimen depending on which has the lower yield stress (σ_y). If the Tresca condition is used, yielding will occur when:

$$\tau_{max} = \frac{\sigma_y}{2} \qquad (A.2)$$

Then from Eqs. A.1 and A.2

$$p = \frac{\sigma_y}{2\sqrt{\left(\frac{k - 1}{2}\right)^2 + \quad ^2}} \qquad (A.3)$$

The two-dimensional plain strain solution for an ideal rigid-plastic material loaded by a flat punch without friction was determined by Prandtl [42], and the value of k during plastic deformation found to be:

$$k = \frac{\pi}{2 + \pi}$$

Assuming this value to approximately represent the stresses ratio at the plastic asperity Eq. A.3 gives:

$$p = \frac{\sigma_y}{2\sqrt{\left(\frac{1}{2+\pi}\right)^2 + \mu^2}} \qquad (A.4)$$

A.2 Cyclic Loading Condition

The shear stress on a general plane AC is given by:

$$\tau_1 = \frac{1}{2}(1 - k)\, p \sin 2\theta - \mu p \cos 2\theta + \frac{\Delta S}{4} \sin 2\theta \quad \left(\text{for } \frac{\Delta S}{2} \text{ tensile}\right)$$

and $$\tau_2 = \frac{1}{2}(1 - k)\, p \sin 2\theta + \mu p \cos 2\theta - \frac{\Delta S}{4} \sin 2\theta \quad \left(\text{for } \frac{\Delta S}{2} \text{ compressive}\right)$$

then $$\Delta\tau = \tau_1 - \tau_2 = \frac{\Delta S}{2} \sin 2\theta - 2\mu p \cos 2\theta$$

It follows that the maximum value of $\Delta\tau$ is given by

$$(\Delta\tau_{max}) = \sqrt{4\,\mu^2\, p^2 + \left(\frac{\Delta S}{2}\right)^2}$$

or rearranging:

$$\frac{\Delta S}{2} = \sqrt{\Delta\tau_{max}^{\,2} - 4\,\mu^2\, p^2} \qquad (A.5)$$

Substituting from A.4 into A.5

$$\frac{\Delta S}{2} = \sqrt{\Delta\tau_{max}^{\,2} - \frac{4\,\mu^2\,\sigma_y^{\,2}}{4\left[\left(\frac{1}{2+\pi}\right)^2 + \mu^2\right]}}$$

$$= \sqrt{\left[\Delta\tau_{max}^{\,2} - \frac{\mu^2\,\sigma_y^{\,2}}{.0378 + \mu^2}\right]}$$

Hence, under the fretting condition, the maximum shear stress range is $\Delta\tau_{max}$ and to initiate a fatigue crack (i.e., $\Delta\tau_{max} = \Delta\tau_{fn}$) this range must be equal to that required under axial loading only ($\Delta\tau_N$)

but $$\Delta\tau_N = \frac{\Delta S_N}{2}$$

Therefore:

$$\frac{\Delta S_{fN}}{2} = \sqrt{\left[\left(\frac{\Delta S_N}{2}\right)^2 - \frac{\mu^2 \sigma_y^2}{.0378 + \mu^2}\right]} \qquad (A.6)$$

This equation can be used to predict the fretting fatigue strength, from the fatigue strength, the coefficient of friction and the tensile yield stress.

APPENDIX B

ANALYSIS OF FRETTING FATIGUE MACROSTRESSES FOR ELASTIC CYLINDRICAL CONTACT

Figure B.1 defines the contact geometry and the analysis assumes:

(i) The coefficient of friction is constant;

(ii) The tangential stress is equal to the normal stress x coefficient of friction;

(iii) The contact pressure distribution is given by the Hertz analysis even in the presence of the tangential force.

Then from Eq. 1

$$p(x) = \frac{\pi}{4} p_{av} \sqrt{1 - \left(\frac{x}{L}\right)^2} \tag{B.1}$$

and from Assumption (ii)

$$\tau(x) = \mu \frac{\pi}{4} p_{av} \sqrt{1 - \left(\frac{x}{L}\right)^2} \tag{B.2}$$

The Smith and Liu analysis gives Eq. 5 for the stresses in the specimen associated with these contact distributions.

In cases where an alternating stress of range ΔS is applied in the x direction, this can be superimposed on Eq. 5 to give, with reference to Fig. B.2:

a. For maximum applied tensile stress

$$\sigma_{xx} = \frac{\Delta S}{2} + \frac{8\mu}{\pi} p_{av} \left(\frac{x}{L}\right) - \frac{4}{\pi} p_{av} \sqrt{1 - \left(\frac{x}{L}\right)^2} \tag{B.3}$$

$$\sigma_{yy} = - \frac{4 p_{av}}{\pi} \sqrt{1 - \left(\frac{x}{L}\right)^2} \tag{B.4}$$

$$\tau_{xy} = \frac{4\mu}{\pi} p_{av} \sqrt{1 - \left(\frac{x}{L}\right)^2} \tag{B.5}$$

b. For maximum applied compressive stress

$$\sigma_{xx} = -\frac{\Delta S}{2} - \frac{8\mu p_{av}}{\pi}\left(\frac{x}{L}\right) - \frac{4}{\pi} p_{av}\sqrt{1 - \left(\frac{x}{L}\right)^2} \tag{B.6}$$

$$\sigma_{yy} = -\frac{4 p_{av}}{\pi}\sqrt{1 - \left(\frac{x}{L}\right)^2} \tag{B.7}$$

$$\tau_{xy} = -\frac{4\mu p_{av}}{\pi}\sqrt{1 - \left(\frac{x}{L}\right)^2} \tag{B.8}$$

On the general plane AC

$$\tau_\theta = \left(\frac{\sigma_{xx} - \sigma_{yy}}{2}\right) \sin 2\theta + \tau_{xy} \cos 2\theta$$

Hence

$$\Delta\tau_\theta = \left[\left(\frac{\sigma_{xx} - \sigma_{yy}}{2}\right)_{\text{tension}} - \left(\frac{\sigma_{xx} - \sigma_{yy}}{2}\right)_{\text{compression}}\right] \sin 2\theta$$

$$+ \left[(\tau_{xy})_{\text{tension}} - (\tau_{xy})_{\text{compression}}\right] \cos 2\theta$$

and substituting from Eqs. B.3 through B.8

$$\Delta\tau_\theta = \left[\frac{\Delta S}{2} + \frac{8}{\pi} p_{av}\,\mu\left(\frac{x}{L}\right)\right] \sin 2\theta + \frac{8}{\pi} p_{av}\,\mu\sqrt{1 - \left(\frac{x}{L}\right)^2} \cos 2\theta$$

$$\Delta\tau_{\theta_{max}} = \sqrt{\left[\frac{\Delta S}{2} + \frac{8}{\pi} p_{av}\,\mu\left(\frac{x}{L}\right)\right]^2 + \frac{64}{\pi^2} p_{av}^2\,\mu^2\left[1 - \left(\frac{x}{L}\right)^2\right]}$$

$$\sqrt{\left(\frac{\Delta S}{2}\right)^2 + \frac{8\,\Delta S}{\pi} p_{av}\,\mu\left(\frac{x}{L}\right) + \frac{16\,\mu^2}{\pi} p_{av}^2}$$

and with respect to x this gives a maximum at x = L

$$(\Delta\tau)_{max} = \left(\frac{\Delta S}{2} + \frac{8\, p_{av}}{\pi}\,\mu\right) \tag{B.9}$$

Then if $(\Delta\tau)_{max}$ initiates fatigue failure we get

$$(\Delta\tau)_{max} = \Delta\tau_{fN} = \frac{\Delta S_N}{2}$$

and

$$\frac{\Delta S}{2} = \frac{\Delta S_{fN}}{2}$$

Hence

$$\frac{\Delta S_{fN}}{2} = \frac{\Delta S_N}{2} - 8\, p_{av} \frac{\mu}{\pi} \qquad \text{(B. 10)}$$

which can be used to predict the fretting fatigue strength.

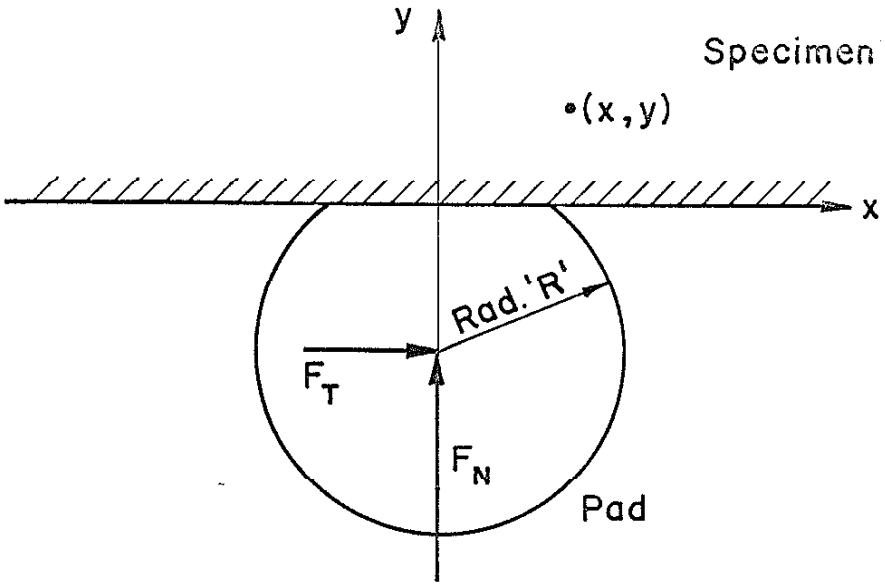

Fig. B1 Cylindrical Contact Geometry

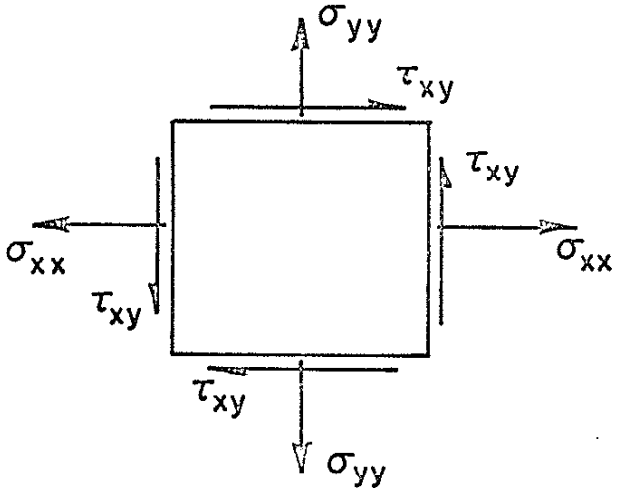

Fig. B2 Stress Notation

APPENDIX C

PHOTOELASTIC ANALYSIS OF CONTACT STRESSES

C.1 Introduction

The analysis was carried out to compare the stress distributions associated with cylindrical and rectangular contact on a flat surface. The geometry was arranged to give equal contact areas under a particular loading so that the results could be compared directly.

C.2 Test Configuration

The photoelastic model and loading arrangement is shown in Fig. C.1. The case shown represents the rectangular contact pads (Item 2). For reasons discussed later, it was found to be advantageous to use pads with two contact points; these were then loaded with normal forces P, applied by loading rings which are not shown.

The tangential load was applied through the tangential load links (Item 4). These were bolted to the steel backing and could be adjusted to ensure that the line of action of the force passed through the contact surface.

The contact pad was mounted on the steel backing using Eastman 910 adhesive.

Care was taken to ensure that the contact surfaces were smooth and clean, and the reproducibility of the fringe patterns showed that the surface preparation was adequate.

C.3 Contact Pad Geometry

Initial experiments, using a single contact on each side of the specimen, indicated that serious errors could be introduced in the local stress distribution if the applied forces were not exactly axial and tangential.

This is shown in Fig. C2(a) where it is apparent that the contact pressure distribution must redistribute to react to the moment $P \times \Delta$. It is also proved difficult

to ensure that the tangential load passed through the contact surface, because deformation of the system under load could alter the initial alignment which was carried out in the unloaded stated.

In order to reduce these errors, the pad with two contact areas, shown in Fig. C2(b), was used. This system reduces the errors discussed above, since moments resulting from imperfect alignment can be resisted by small changes in contact stress multiplied by the relatively large moment arm 's'. With this arrangement, it proved relatively simple to obtain reproducible symmetrical fringe patterns due to normal loading.

The disadvantage of the system was that some stress interaction occurred between contact pads. However, by using pads with the contacts three inches apart, this effect was found to be small.

C.4 Material Selection

In order to compare the results for cylindrical and rectangular pads, it was considered advantageous to use equal contact areas under reasonable magnitudes of normal force.

Expressions from the Hertzian theory for the contact area of a cylinder on a flat plate were used to give a relationship between: normal force, radius of curvature of the cylinder, and the elastic properties of the materials. This approach was further limited by the fact that it proved difficult to obtain accurate radii above about ten inches.

From preliminary calculations, it was found that using normal photoelastic materials contact lengths of .25 in. appeared feasible with a radius of 6 in. and normal forces of 150 lbf. A trial and error procedure was then adopted using CR 39, Castolite and Homolite. Mechanically, CR 39 met the requirements most closely; however, photoelastically, the time edge exhibited by this material proved a serious problem. Eventually it was decided to compromise and Homolite was used for specimen and pad.

A contact length of .25 in. was obtained using a normal force of 167 lbf and a radius of 5.5 in.

A further problem arose because the coefficient of friction for the photoelastic materials was found to vary between .25 and .3, whereas for the steel used in the fretting test it is approximately .6 [36]. No way could be found to compensate for this difference, and it was decided to continue with the test program and bear this error in mind when analyzing the results.

C.5 Test Procedure

The rectangular and cylindrical pads were loaded normally with forces 167 and 250 lb. The maximum tangential force which could be supported without general slip was then applied. The isochromatic fringe pattern was recorded photographically in each case.

In addition, the rectangular contact was analyzed in more detail, isoclinics were recorded and the fringe order determined around a rectangular boundary using Tardy compensation.

Material calibration was carried out using a tensile specimen having three different cross sections as recommended by Frocht [37].

C.6 Experimental Results

The photographic records of the isochromatics are presented in Figs. C3 through C5. The material calibration was 280 lb/in.^{2} shear for one fringe.

C.6.1 Cylindrical Contact

The effect of the tangential force is shown in Fig. C5(a) and the integral and half order fringes sketched in Fig. C6. Smith and Liu's analytical results are compared with the experimental values in Fig. C7.

Figure C8 shows the maximum shear stress variation along lines perpendicular to the specimen surface at the edge of the contact area (x_1 and x_2 in Fig. C6).

The agreement between experimental and theoretical results in Fig. C7 suggests that the assumptions of the analytical treatment are justified.

If the tangential force is reversed as is the case in fretting, material at similar points along x_1 and x_2 is cycled between the shear stress limits shown in Fig. C8. It can be seen that appreciable stress amplitudes occur over a depth $x/a = 1$.

C.6.2 Rectangular Contact

The shear stress distribution, resulting from normal and tangential forces on the rectangular contact, is shown in Fig. C5(b) and the integral and half order fringes sketched in Fig. C9. There is seen to be an increase in the stress concentration at one edge of the contact area and a decrease at the other.

The extent of this change is shown in Fig. C10, which gives the variation in maximum shear stress along lines perpendicular to the specimen surface through the edges of the contact.

C.7 Discussion

The photoelastic analysis gives a good qualitative understanding of the stress distributions associated with the two-contact geometries investigated. It can be seen that, under normal loading only, the stresses associated with the cylindrical and rectangular pads differ markedly. The effect of superimposing a tangential force has a similar result in both cases in that it causes an increase in the stress at one edge of the contact area and a decrease at the other. In both cases the high local stress extend over a depth of material of the order of one quarter the contact length.

Quantitatively, the results show that for normal loading the maximum shear stresses in the cylindrical contact is approximately .4 of the mean normal pressure, which agrees well with the analytical results of Smith and Liu. Superposition of the tangential force does not significantly change the magnitude of this maximum stress, however, it causes the stress distribution to become asymmetric.

The maximum stress associated with the rectangular contact cannot be determined from the photoelastic analysis because of the high stress concentration at the edge of the contact area. The stress magnitudes away from these points are, however, clearly defined.

C.7.1 Application to Fretting

In the initiation of fatigue cracks, there are two important criteria:

a. The change in shear stress magnitude, which occurs when the tangential force is reversed, and

b. The volume of material, which is subjected to this cyclic shear stress.

The photoelastic results can be used to give some indication of these two factors. Considering material at the edge of the contact area extending to depths $x/L = .1$ and $.033$. The shear stress variation ($\Delta\tau$) caused by reversing the tangential force is:

	Range of Shear Stress $\Delta\tau$	
	$\frac{y}{L} = .033$	$\frac{y}{L} = .1$
Cylindrical	$.15\ p_{av}$	$.3\ p_{av}$
Rectangular	$>.6\ p_{av}$	$.6\ p_{av}$

This difference suggests that the rectangular contact should be more detrimental in causing fretting fatigue damage.

Two important areas which have not been considered in this analysis and where additional work is required are discussed below.

C.7.2 Relative Movement

In actual fretting situations relative movement occurs between the contact and the specimen. The stress distributions, determined in this experimental analysis,

will be set up each time the motion is reversed. It seems possible, that as these represent limiting friction conditions, the stresses determined may represent the maximum; however, other factors are involved in the dynamic situation such as stick-slip phenomenon.

C.7.3 Coefficient of Friction

The stress distributions determined apply only to the case where the coefficient of friction is .3. Higher values would allow larger tangential forces to be applied which would result in larger shear stress amplitudes.

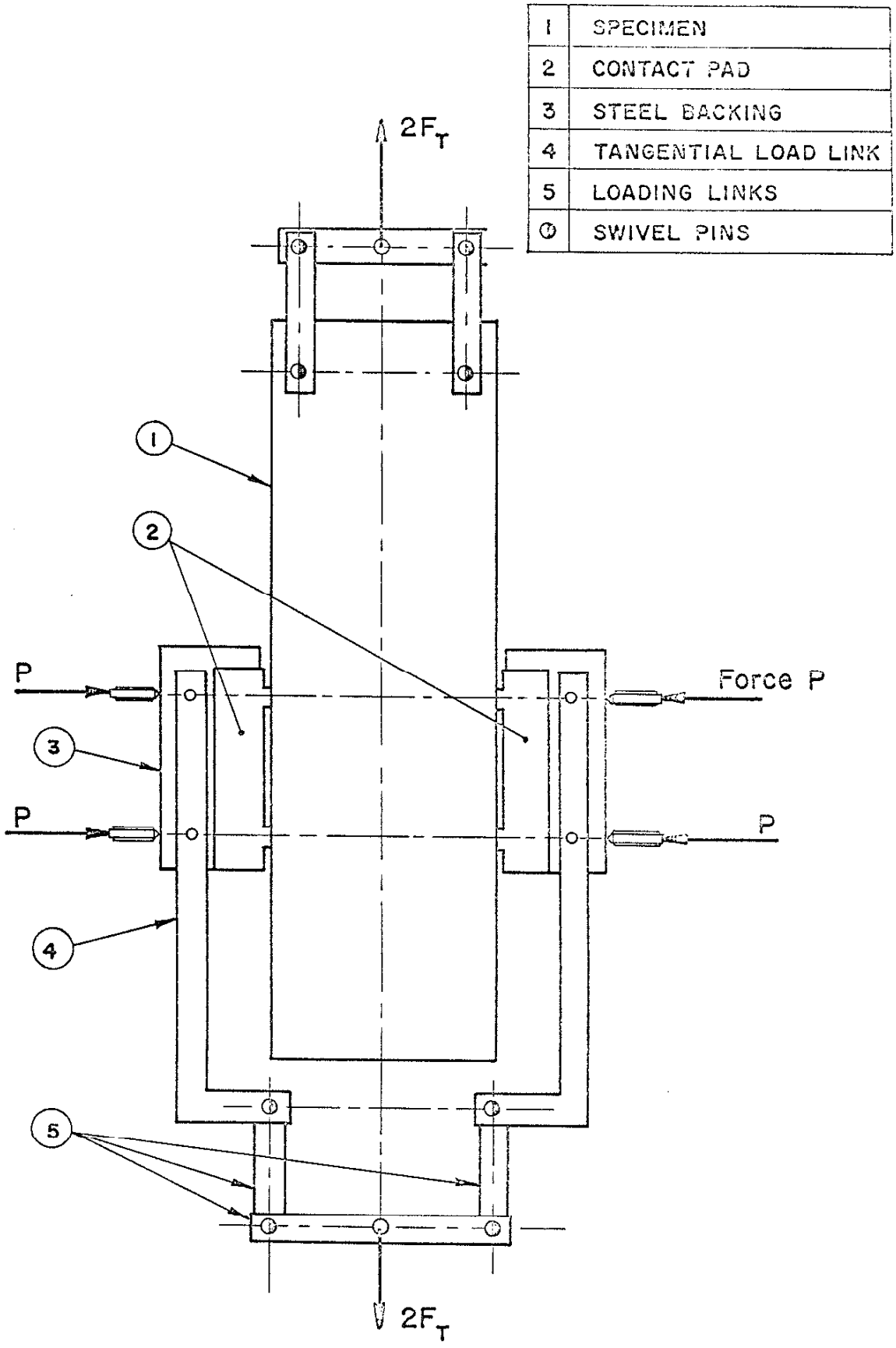

Fig. C1 Photoelastic Test Rig

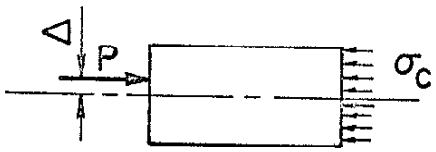

Fig. C2(a)

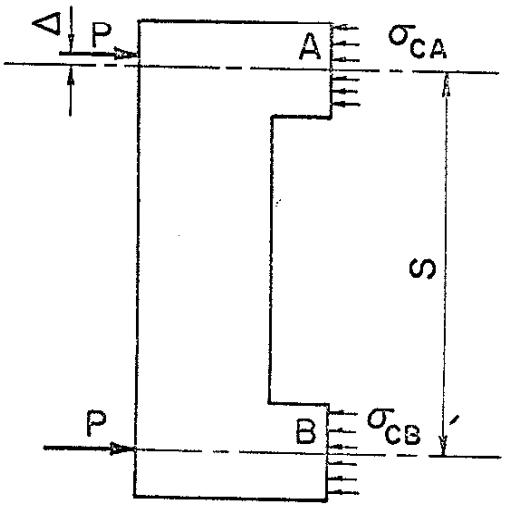

Fig. C2(b)

Fig. C2 Effect of Force Eccentricity

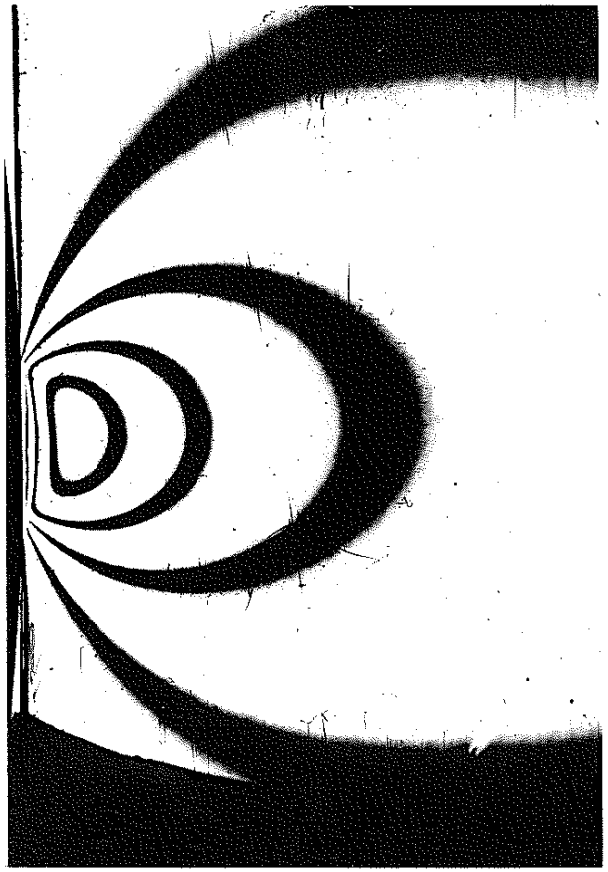

a) Cylindrical Contact

Normal Force - 167 lb
Tangential Force - 0

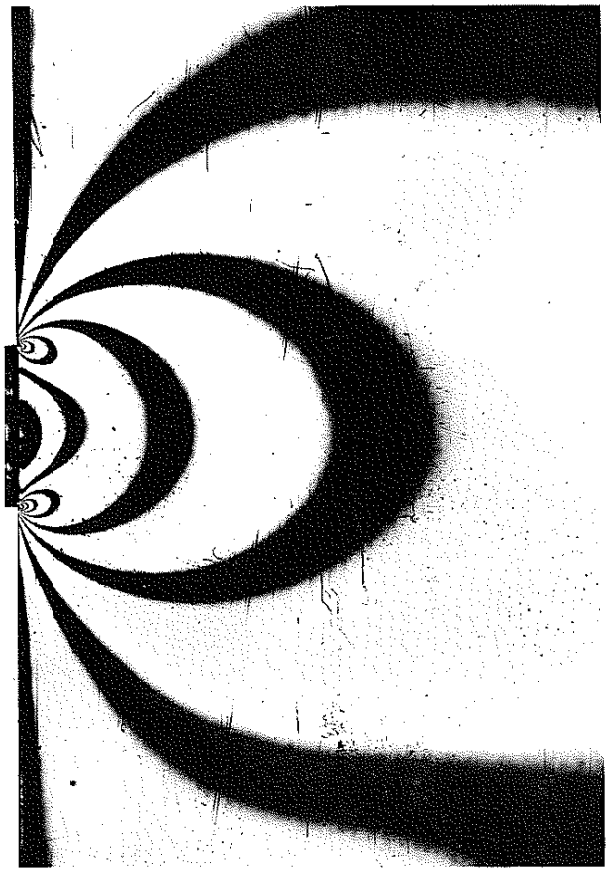

b) Rectangular Contact

Normal Force - 167 lb
Tangential Force - 0

FIGURE C-3. PHOTOGRAPHS OF ISOCHROMATICS

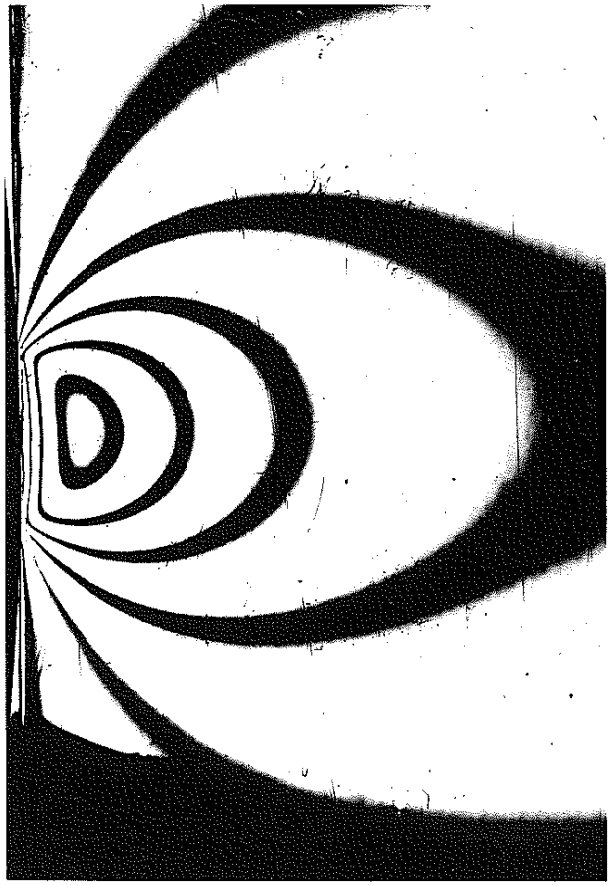

a) Cylindrical Contact

Normal Force - 250 lb
Tangential Force - 0

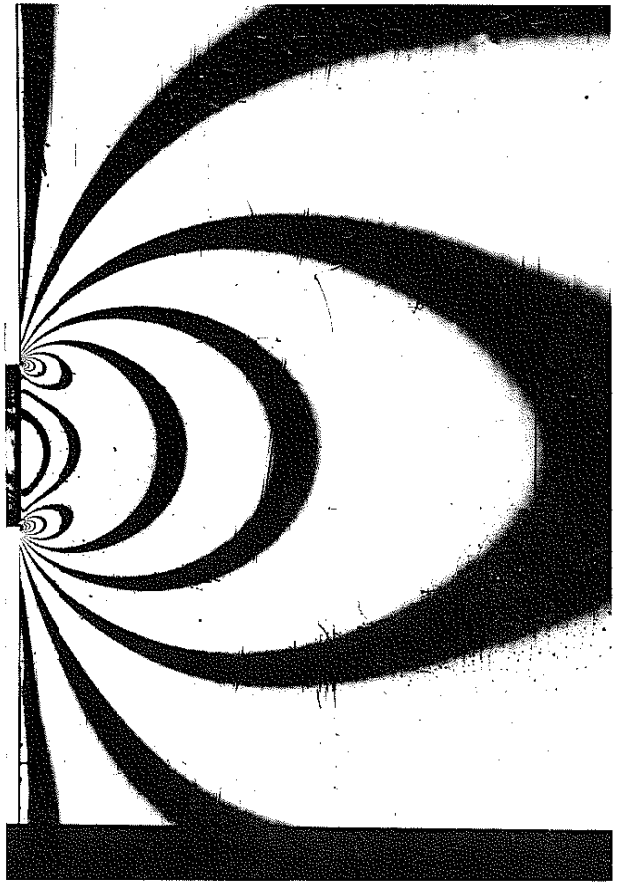

b) Rectangular Contact

Normal Force - 250 lb
Tangential Force - 0

FIGURE C-4. PHOTOGRAPHS OF ISOCHROMATICS

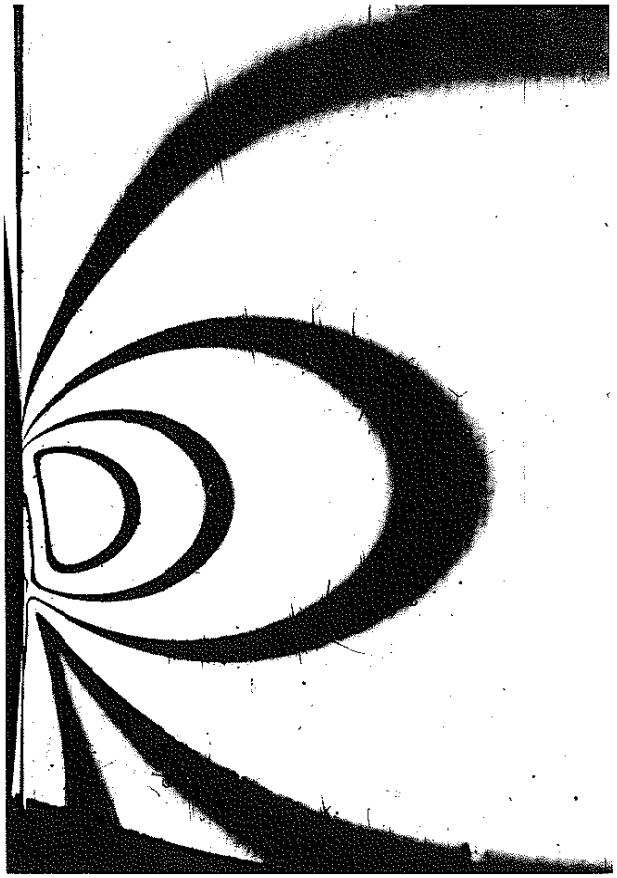

a) Cylindrical Contact

Normal Force - 167 lb
Tangential Force - 55 lb

b) Rectangular Contact

Normal Force - 167 lb
Tangential Force - 55 lb

FIGURE C-5. PHOTOGRAPHS OF ISOCHROMATICS

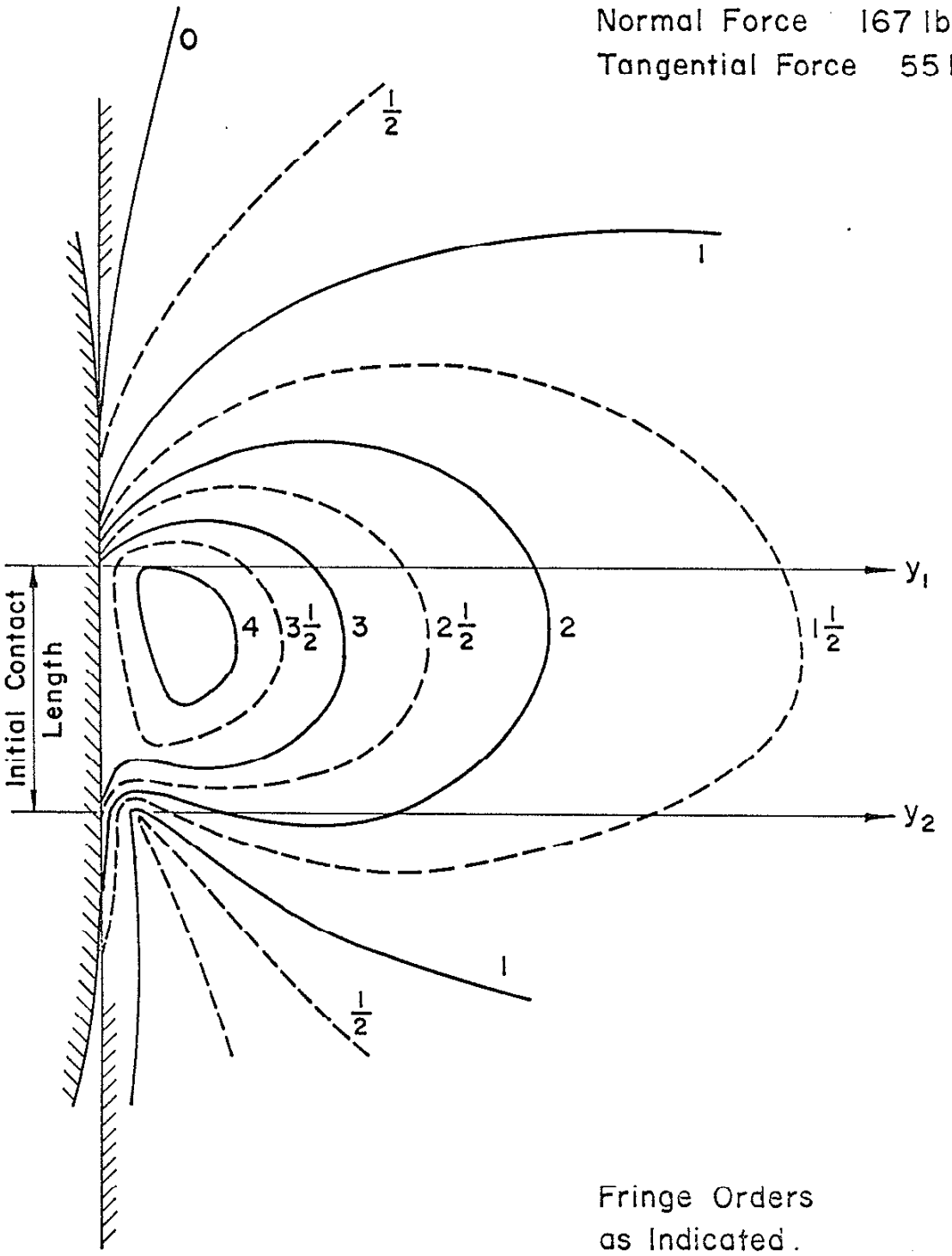

Fig. C6 Cylindrical Contact, Isochromatic Fringes

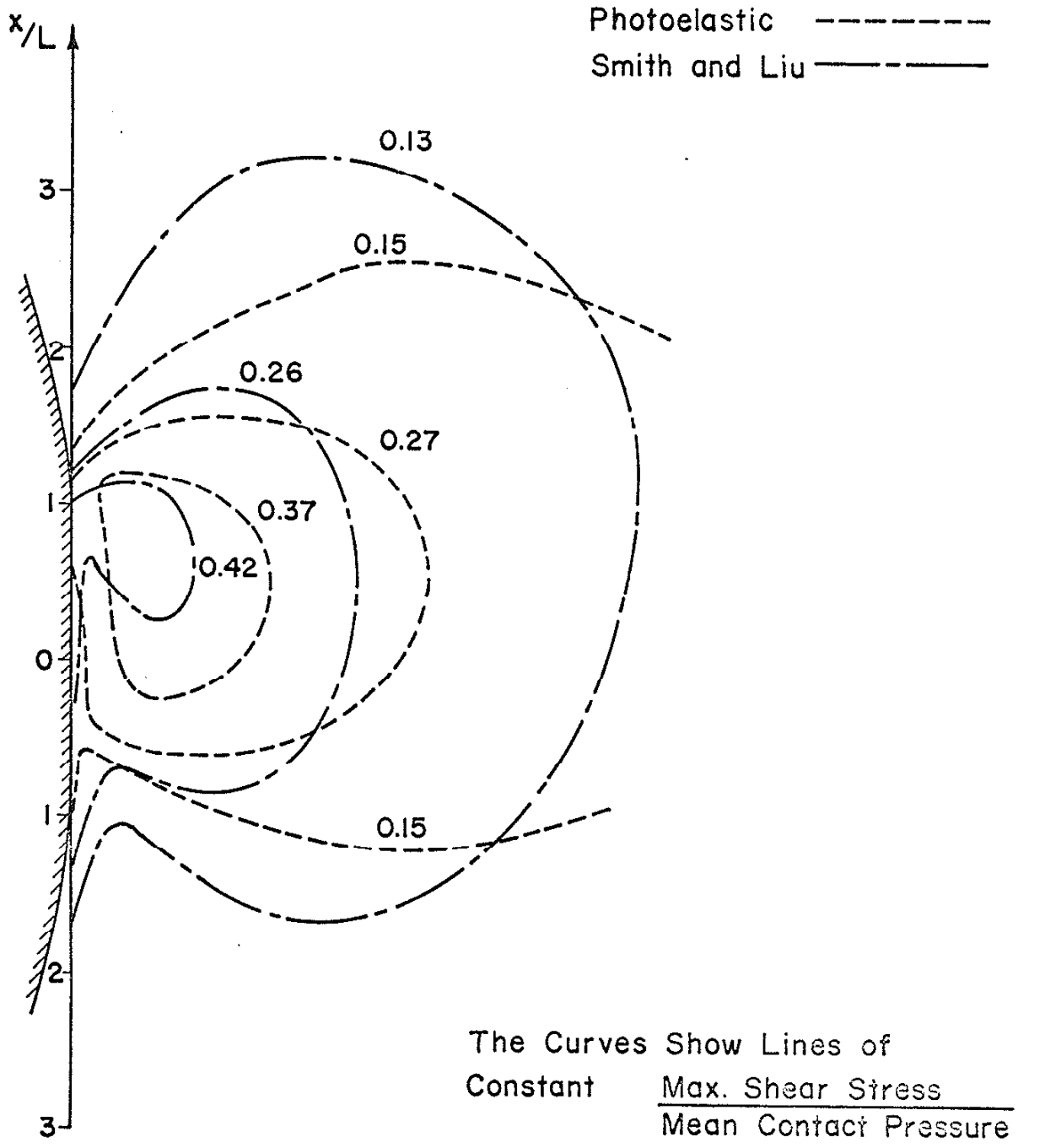

Fig. C7 Cylindrical Contact, Comparison of Theoretical and Photoelastic Results

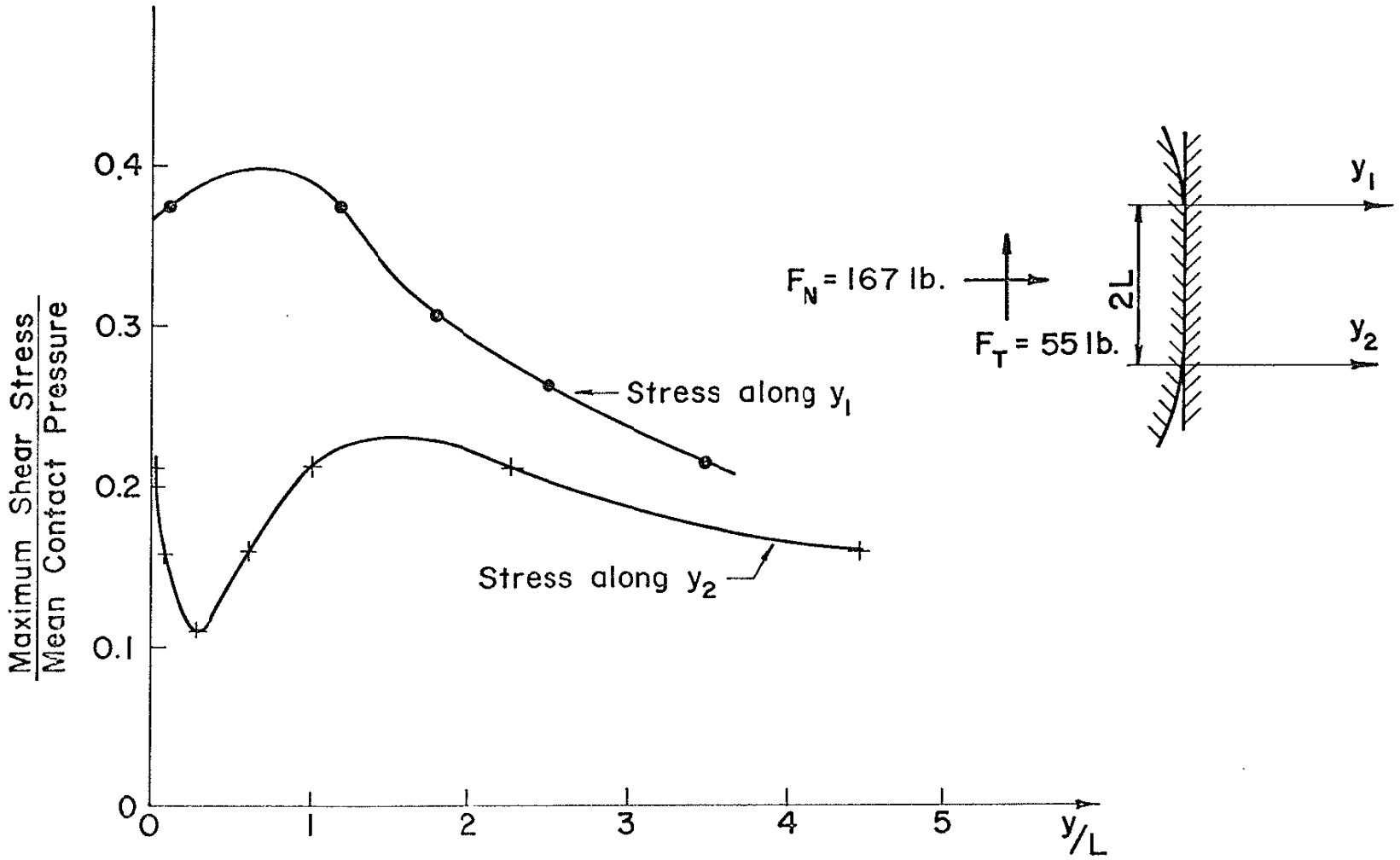

Fig. C8 Cylindrical Contact — Maximum Shear Stress Distribution

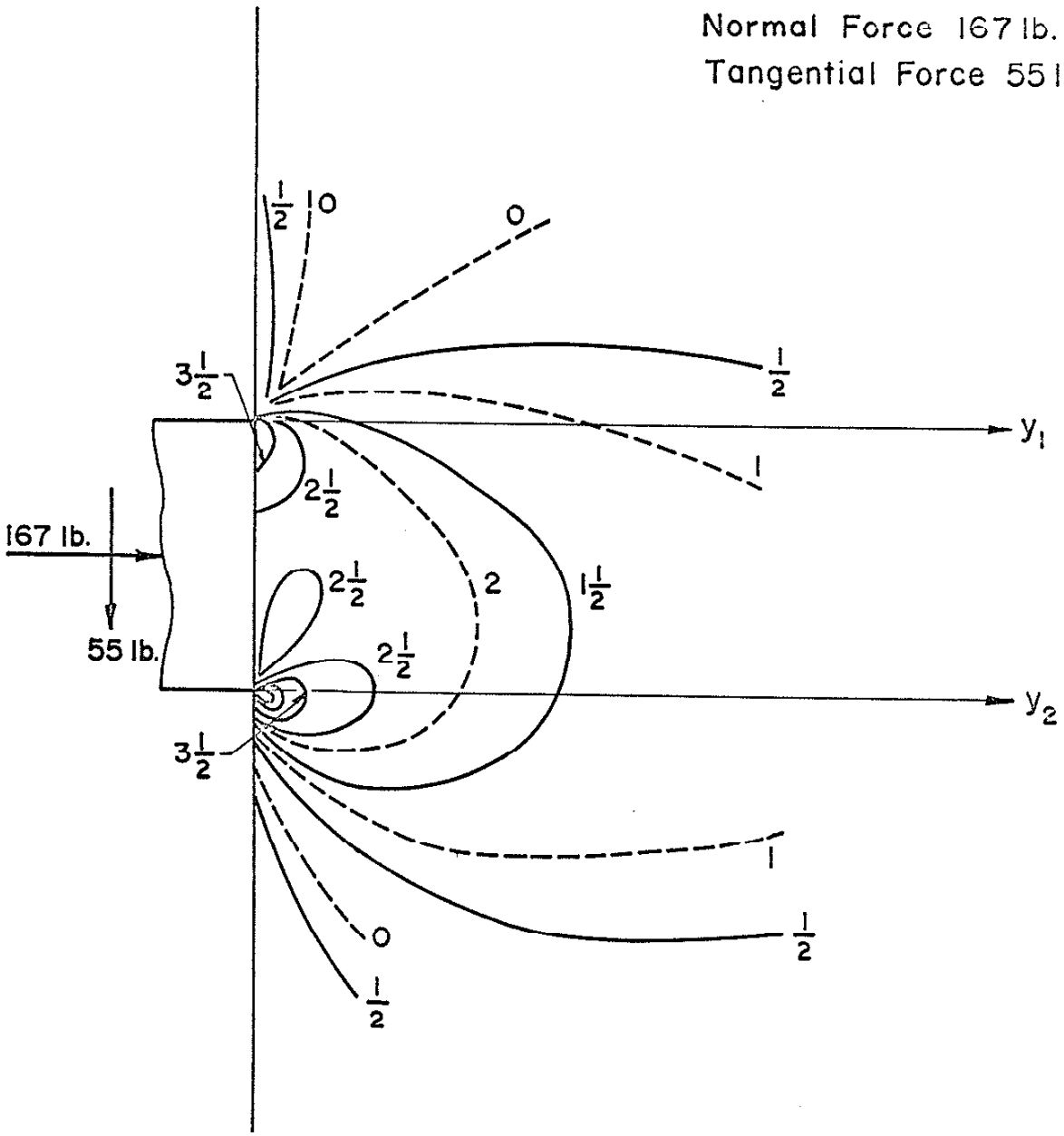

Fig. C9 Rectangular Contact — Isochromatic Fringes

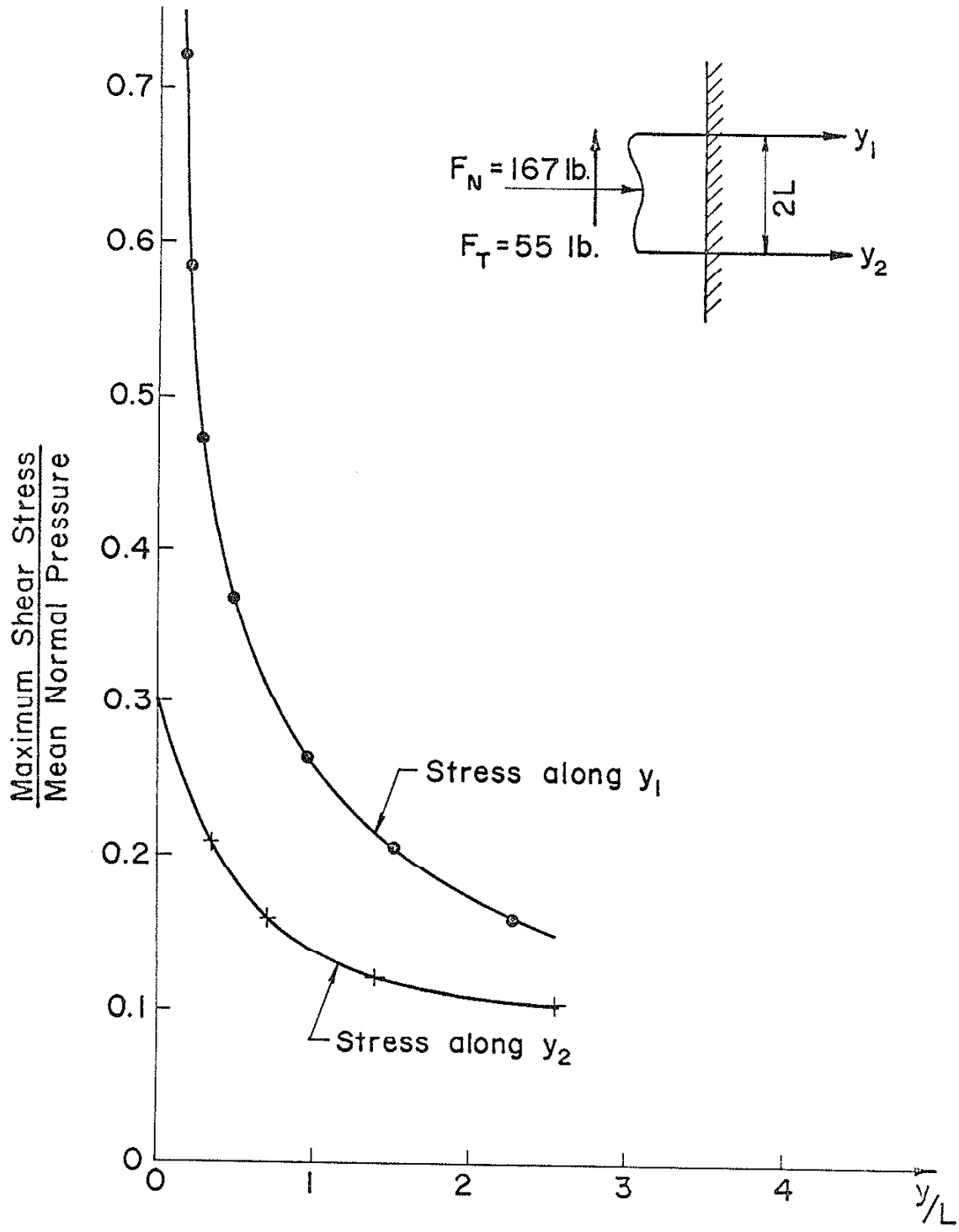

Fig. C10 Rectangular Contact —
Maximum Shear Stress Distribution